INELASTIC BENDING CAPACITY IN COLD-FORMED STEEL MEMBERS

report to:
American Iron and Steel Institute
Committee on Specifications
Subcomittee 10 – Element Behaviors and Direct Strength Method
Subcomittee 24 – Flexural Members

report prepared by
Yared Shifferaw
(Ben Schafer – Advisor)
Thin-walled Structures Research Group
Department of Civil Engineering
Johns Hopkins University

July 2008

JOHNS HOPKINS
ENGINEERING

Department of Civil Engineering
The Johns Hopkins University
3400 N. Charles Street
Baltimore MD 21218-2686
(410) 516-8680 / FAX (410) 516-7473

Ben Schafer, Ph.D., P.E.
Associate Professor
203 Latrobe Hall
410-516-7801
schafer@jhu.edu

To: Helen Chen, Senior Engineer
Cold-Formed Steel Construction
American Iron and Steel Institute
1140 Connecticut Ave. - Suite 705
Washington, DC 20036
email: hchen@steel.org

re: AISI report on Inelastic Bending of Cold-Formed Steel Members

Helen

The enclosed research report has been prepared for the AISI as supporting material for proposed additions to the AISI Specification (AISI-S100-07) with respect to inelastic bending of cold-formed steel flexural members. In particular, an extension to the Direct Strength Method of Appendix 1 of AISI-S100-07 is proposed which allows for design capacities to exceed M_y (and approach M_p) as a function of the slenderness in the local-global or distortional modes.

The funding for this project largely came from the National Science Foundation, and journal publications related to this work are in preparation. For now, we felt that this AISI report would be the best way to share the work with the AISI-COS committee and to help the committee proceed with creation of a ballot.

Sincerely,

Ben Schafer

Table of Contents

1. Introduction.....5

1.1 Introduction.....5
1.2 Elementary Mechanics for Inelastic Reserve 6
1.3 Mechanisms for Inelastic Reserve 8
1.4 Existing Tests and Finite Element Models 9

2. Development and Verification of Unique and Simple Finite Element Model to Study Local and Distortional Inelastic Bending Capacity 13

2.1 Material Model.....13
2.2 Element and Mesh Density 14
2.3 Solution Controls.....15
2.4 Boundary Condition 16
2.4.1 Test Boundary Conditions 16
2.4.1.1 Local Tests.....16
2.4.1.2 Distortional Tests 17
2.4.2 Idealized FE model boundary conditions.....18
2.5 Imperfection 21
2.6 Verification of FE Models.....21
2.7 Conclusion 24

3. Comprehensive Finite Element Study 25

3.1 Member Length for Local Finite Element Model 26

3.1.1Study of Mesh Density and Imperfection Sensitivity on Member Length Selection 26

3.2 Member Length for Distortional Finite Element Model.....28

3.2.1 Study of Mesh Density and Imperfection Sensitivity on Member Length Selection 28
3.2.2 Study on the Impact of Lateral-Torsional Buckling in Selection of Member Length for Distortional Models 33

4. Parametric Study and Design Formulations 37

4.1 Slenderness vs. Strain Limit Ratio 39
4.1.1 Parametric Study 39
4.1.2 Design Equations 41
4.2 Strain Limit vs. Strength 46
4.2.1 Parametric Study 46
4.2.2 Design 47
4.3 Direct Strength Method Formulation: Slenderness as a Function of Strength 49
4.3.1 Parametric Study 49
4.3.2 Design 50
4.3.3 Design Statistics 52

5. Appendix 53

Acknowledgement 62

References 62

1. INTRODUCTION

1.1 Introduction

It is common for braced hot-rolled steel beams to develop bending capacity exceeding the first yield moment, M_y, and reaching as high as the plastic moment, M_p, depending on the constituent elements' slenderness. In the case of cold-formed steel (CFS) such inelastic reserve (capacity exceeding M_y) is uncommon in comparison with those of hot-rolled steel cross-sections. This is due to the thin-walled nature of cross-sections inducing the limit states of local, distortional, and/or global buckling and hence reducing the bending capacity to be lower than the yield moment. However, in practice, inelastic reserve capacity has been found to develop in tests carried out on cold-formed steel thin-walled beams.

Research was done on inelastic reserve capacity of cold-formed steel beams by Reck, et. al as early as 1975 who investigated CFS beams with web-stiffened compression flanges for inelastic reserve strength. Different test specimens were studied and included sections with initial yielding in compression, in tension as well as balanced ones. The results of these tests indicated that the ratio of the compressive strain to yield strain (C_y) was a function of the compressive flange's width to thickness ratio. A design curve relating C_y to that of the compressive flange's width to thickness ratio and also modified to include the effect of yield stress was developed. Reck et al. (1975) also discussed the hot-rolled steel provisions, but noted differences between CFS and hot-rolled sections: higher web to flange area, greater use of unsymmetric sections resulting in first yield occurring

in the tension flange, and the inability of CFS sections to sustain high compressive strains. Through testing, provisions for the maximum compressive strain that stiffened CFS elements could sustain, predicted as a function of element slenderness, were developed (Yener and Peköz 1983, 1985) and adopted as may be found in current CFS specifications (NAS 2001). Bambach and Rasmussen (2004) extended the NAS (2001) approach to cover inelastic reserve for unstiffened elements under a stress gradient with the free edge in tension.

Although recent research has been conducted on inelastic reserve and ductility in hot-rolled steel beams (primarily for seismic applications) inelastic reserve has not been studied further for CFS beams. The extent to which inelastic reserve exists in commonly used CFS sections, and the typical increases one achieves in capacity are not widely known. Existing design provisions do not apply to the most commonly used beams (C's and Z's) and the new Direct Strength Method (DSM) (Schafer 2006, NAS 2004 Appendix 1) has not been extended to cover inelastic bending reserve.

1.2 Elementary Mechanics for Inelastic Reserve

The moment in a cross-section may be readily determined by the integration of the longitudinal stress, σ, times the distance from the neutral axis, y, over the cross-section, A, via

$$M = \int_A \sigma y dA \qquad (1)$$

The neutral axis location from the bottom of the section, y', may be determined for a cross-section of depth, h, by enforcing equilibrium via

$$\int_0^{y'}\int \sigma dx dy + \int_{y'}^{h}\int \sigma dx dy = 0 \qquad (2)$$

Now, consider a nonlinear (uniaxial) material, where the stress is a function of the strain, but still assuming elementary mechanics where the strain varies linearly across the section:

σ = f(ε) and σ = (y/y_{lim}) ε_{max} (3)

where y_{lim} is the maximum distance to the extreme fiber of the cross-section from the neutral axis, i.e., y_{lim}= max(y', h-y'), and ε_{max} is the strain sustained at that location. The moment M is then

$$M = \int_A f(\varepsilon) y dA = \int_A f((y/y_{lim})\varepsilon_{max}) y dA \qquad (4)$$

Thus, the moment in the section is a function of the maximum strain sustained. For uniaxial treatment of an elastic-perfectly plastic material

f(ε) $\equiv \sigma$ = Eε for $\varepsilon < \varepsilon_y$ and $\sigma = f_y$ for $\varepsilon > \varepsilon_y$ (5)

So, for the case of $\varepsilon_{max} = \varepsilon_y$, we have the classic moment at first yield:

$$M_y = \int_A E((y/y_{lim})\varepsilon_y) y dA = \int_A E\varepsilon_y / y_{lim}\, y^2 dA = f_y I / y_{lim} = f_y S \qquad (6)$$

Further, for the case $\varepsilon_{max}=\infty$

$$M_p = \int_A f_y y dA = f_y Z \qquad (7)$$

In general for $\varepsilon_y < \varepsilon_{max} < \infty$ the moment follows Eq. 4. Note, that Eq. 2 must be enforced uniquely for each ε_{max} to determine the current neutral axis location (y'). CFS sections have some inelastic reserve capacity, but typically not M_p; hence the

moment sustained is determined by the maximum strain, typically defined in terms of the yield strain:

$$\varepsilon_{max} = C_y \varepsilon_y \quad (8)$$

Depending on the cross-section geometry first yield may be in tension or compression and thus we may define the maximum strains as:

$$\varepsilon_{max\text{-}compression} = C_y \varepsilon_y \text{ and } \varepsilon_{max\text{-}tension} = C_{y\text{-}tension} \varepsilon_y \quad (9)$$

where typically the concern is with compressive strains, and thus the maximum C_y that can be sustained before inelastic buckling.

1.3 Mechanisms for Inelastic Reserve

CFS beams achieve inelastic bending reserve through two, primarily distinct, mechanisms. First, for cross-sections which are symmetric about the axis of bending, or have first yield in compression, inelastic reserve is achieved through the ability of the cross-section to sustain higher compressive strains (C_y>1) before inelastic local, or distortional buckling occurs. The evolution of stress through the cross-section for sections symmetric about the axis of bending is illustrated in Figure 1(i). The second inelastic reserve mechanism is for sections with first yield in tension, the greatest portion of inelastic reserve is achieved through yielding in the tension flange of the section ($C_{y\text{-}tension}$>1) and subsequent shift in the neutral axis, as illustrated in Figure 1(ii). If the compressive fiber (top of Figure 1(ii)) does not yield (i.e., Figure 1(ii.b)) then all of the inelastic reserve generates from tension yielding; however, if high enough rotations are sustained, some yielding in compression may occur – and thus at least partial inelastic buckling may be

sustained. This work largely focuses on the first mechanism: inelastic buckling in symmetric sections.

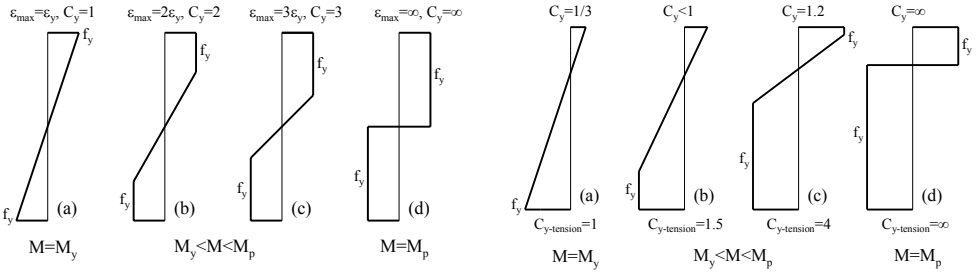

(i) symmetric section (ii) first yield in tension

Figure 1 Evolution of stress in bending following elementary mechanics for an elastic-perfectly plastic material

1.4 Existing Tests and Finite Element Models

A number of researchers have tested cold-formed steel (CFS) beams for bending resistance. Data was compiled on CFS tests that exhibited inelastic reserve. The sections that were considered mainly included hat and deck sections, and C and Z sections. JHU-Tests in bending of CFS beams of C and Z sections by Yu and Schafer (20003, 2006) separately achieved distinct local and distortional buckling limit states. These test results were used to validate the direct strength method of design, particularly for distortional buckling. Figure 2 shows the test results that were used in DSM development. It can be seen that quite a significant number of these tests lie above the plateau line highlighted on Figure 2 (M_{test} / M_y) which indicates that they possess inelastic reserve bending capacity[1]. The number of

[1] Yield stresses used in the calculations were from the as-formed cross-sections (as opposed to the virgin or coil yield stress), as reported by the various researchers. Thus, it is believed that the majority of capacity above M_y comes from inelastic reserve, not from cold-work of forming effects.

such tests that exhibited inelastic reserve capacity served as a motivation to extend the Direct Strength Method to take into account such additional capacity.

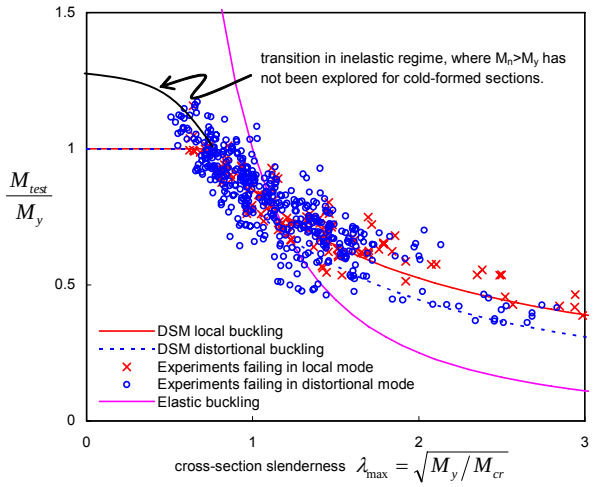

Figure 2 Development of DSM expressions for local and distortional buckling of beams with possible inelastic transition curve highlighted.

Tests resulting in failure bending capacity 95% or higher than the yield moment were selected to closely examine inelastic bending capacity in cold-formed steel beams. The study of these cross-sections indicated that there were distinct mechanisms by which cold-formed steel beams develop inelastic reserve. A summary of the tests that were adopted in this study is given by Table 1. Inelastic capacity was observed in more than 15% of all tests that were considered, which underscores the importance of understanding inelastic reserve in cold-formed steel beams. Maximum observed inelastic reserve was 18%, observed in tests carried out by Yu and Schafer (2003, 2006), with an average maximum reserve of 10%.

After determining the plastic moment of the cross-sections in these tests the shape factors (M_p / M_y) were computed and are given in Table 1. It can be noted that

there is a large variation of shape factors and that the maximum shape factors are significantly higher than the maximum observed inelastic reserve in the tests. Thus, it is clear that partial reserve is achieved, but not the full inelastic bending capacity M_p.

Table 1 Observed inelastic reserve in CFS beams

Section and Researcher	count $M_{test}>0.95M_y$	max M_{test}/M_y	min M_p/M_y	max M_p/M_y
Hats and Deck Sections				
Acharya (1997)	12	1.04	1.10	1.31
Desmond (1977)	2	1.01	1.25	1.25
Hoglund (1980)	36	1.16	1.15	1.26
Papazian (1994)	8	1.12	1.13	1.29
Winter (1946)	3	1.15	1.28	1.32
C and Z Sections				
Cohen (1987)	7	1.05	1.24	1.26
LaBoube and Yu (1978)	10	1.04	1.14	1.19
Rogers (1995)	17	1.15	1.16	1.31
Shan (1994)	6	1.17	1.15	1.23
Yu and Schafer (2003)	8	1.18	1.14	1.20
Yu and Schafer (2006)	4	1.06	1.14	1.23

Further examination of the strain at failure of these tests revealed three regions of failure in bending, as shown in Figure 3. The plot shows failure mechanisms of the cold-formed steel beam tests with respect to normalized ratios of maximum tensile and compressive strain to yield strain. Figure 3 shows tests that fall in the first region which showed no inelastic reserve, those that fall in the second region failed by tension yielding without the compressive fibers reaching yield and the rest of the tests that failed with the compressive fibers subjected to maximum strains exceeding the yield strains. The case of failure by the maximum compressive strain exceeding yield induces inelastic buckling, though first yield could be either in tension or compression.

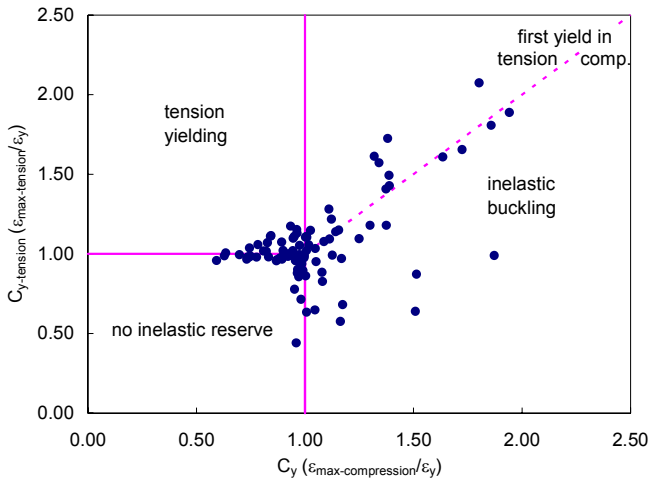

Figure 3 Examination of strain at failure in tests of Table 1

In addition to the actual tests that were carried out, results of Yu and Schafer's (2007) finite element models that were developed for test verification and further extended for use in the study of distortional and local CFS beam bending capacities were used in the study of inelastic reserve capacity reported here. These FE models were used to predict separate local and distortional bending capacities for typical C and Z sections.

2. DEVELOPMENT AND VERIFICATION OF UNIQUE AND SIMPLE FINITE ELEMENT MODEL TO STUDY LOCAL AND DISTORTIONAL INELASTIC BENDING MOMENT

Based on the observation of the existence of inelastic reserve in CFS beams during tests, further investigation was needed to develop finite element analysis models that will capture such behavior and satisfactorily represent actual physical test conditions. With the view to developing a Direct Strength Method approach to investigate inelastic reserve bending capacity in CFS beams unique finite element models were required to actually represent buckling limit states which induce distinct mechanisms for inelastic reserve. Yu and Schafer (2007) tests that were carefully set-up to result in the separation of the distortional and local buckling limit states served as a basis for determining the modeling assumptions in the finite element models to be developed.

2.1 Material Model

In the finite element models that were developed, five different non-linear material models were used. The yield stresses in the material models varied between 33 ksi and 73.4 ksi. Figure 4 shows the stress-strain plots of the material models. The material models were adopted from a series of tensile coupon tests of specimens of the tested cross-sections (Yu and Schafer (2007)). The use of these actual non-linear material models, and not assumed material models, and the observation of inelastic reserve during the tests implied that the phenomenon of inelastic bending in cold-formed steel beams is a real possibility.

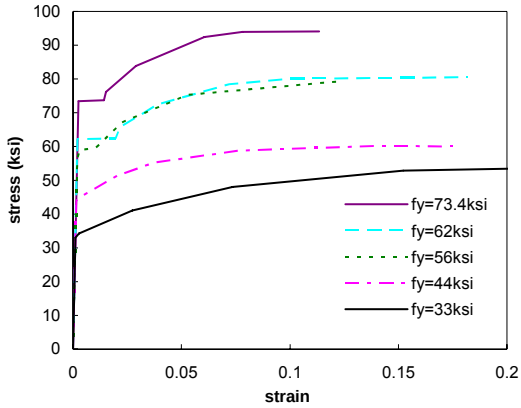

Figure 4 Stress-strain relations used in FE study

2.2 Element and Mesh Density

The nine-node quadratic interpolated thin shell ABAQUS element: S9R5, was used in the analysis. The impact of mesh density was studied by considering the non-linear finite element analysis results with different choice of element aspect ratios. The decision to consider the different aspect ratios was found to be important with respect to the non-linear finite element runs. Not-sufficiently fine meshes coupled with the geometric and material nonlinearities might pose problems of instabilities and/or non-convergence in the numerical solution. Various mesh densities for the different elements of the sections (with respect to flange, web, and corner) were investigated as to the impact on the failure inelastic bending capacity. The mesh density impact analysis was done in both the verification and further parametric studies. Element aspect ratios were kept near 1.0, with the exception being the rounded corner regions where ratios were kept below 4:1. A minimum of 2 elements were employed in the lip, 4 in the flange, and 16 in the web, of the

modeled C and Z sections. Examples of converged meshes are provided in the subsequent sections.

2.3 Solution Controls

The modified Riks method implemented in ABAQUS version 6.7.1 (ABAQUS 2007) is the algorithm adapted to study post-buckling response. In this method nodal variables and the loading parameter define the single equilibrium path, and the solution development requires this path be traversed as far as required. The increment size is limited since at any time there is a finite radius of convergence in the basic Newton method algorithm and path-dependent response is exhibited by most materials and loadings of interest. In the implementation in ABAQUS, a given distance is traversed along the tangent line to the current solution point, and equilibrium is sought in the plane passing through the resulting point and orthogonal to the tangent line.

Different non-linear finite element models were built to study the effect of the various “RIKS” parameters before verification with the tests that were done at Hopkins. The different studies that were conducted included parameter studies such as the impact of initial step increment, the total period, minimum as well as maximum step sizes in the choice of RIKS solution parameters. In the subsequently reported results sufficiently small initial and maximum step sizes were selected, such that peak load typically occurred in approximately 20 steps.

2.4 Boundary Condition

The study of the boundary conditions for the local and distortional buckling modes was found to be the most crucial step in the development of FE models. To achieve separation of these modes, simplified boundary condition approximations resembling the test set-up conditions of Yu and Schafer (2003, 2006) were adopted. The impact of these boundary condition approximations was examined in comparison to the actual test results. The results indicated that the boundary conditions that should be adopted for the local and distortional mode studies were quite different as the two dominant modes represent different deformation in the buckling of the cross-section. Hence, the choice of the boundary conditions for the two cases was based on the general deformed shape of the cross-section where one of the two buckling modes dominated.

2.4.1 Test Boundary Conditions

2.4.1.1 Local Tests

In the set-up for local buckling tests (Yu and Schafer 2003), two members are placed side by side with opposing in-plane flange rotations inducing tension on panel on top (Figure 5.a). The panel thereby provides additional restraint on the flange distortional buckling. In order to engage the panel, closer spacing of fasteners than the standard fastener-panel configuration needed to be used for restricting the flanges from translation.

2.4.1.2 Distortional Tests

In the set-up for distortional tests, two members are placed side by side as in the case of local tests except the panels are removed in the middle span so as to induce such buckling as shown in Figure 5.b.

a.

b.

Figure 5 Yu & Schafer Test set-ups a) Local, b) Distortional

2.4.2 Idealized FE model boundary conditions

A segment of the beam under constant bending was considered in the model to study inelastic bending capacity. Hence corresponding boundary conditions of the idealized model with respect to end restraints needed to effectively capture the continuity conditions in the actual beam and need to be carefully investigated.

In the case of the local buckling FE models, mid-points of the top flange were restrained from rotating, thus simulating an ideal version of the panel restriction of the compression flange in the test set up condition (Figure 5.a). The end boundary

conditions were modeled in two ways for comparison with tests: with rigid boundary condition restraining the ends from warping and, with warping free conditions.

With respect to the distortional buckling mode boundary conditions, two types of boundary conditions were investigated as to the appropriateness and proximity to possible test boundary conditions. The first boundary condition that was considered is similar to the CUFSM boundary conditions where warping is free at the end of the member and restrained in the middle of the member. In this boundary condition the member was also restrained from transverse translations at the ends. It is to be noted that such boundary condition resembling CUFSM boundary conditions represent a pin-ended, but warping-free, condition at the ends. But as can be seen from the experimental setup (Figure 5.b) where the interior top panel was removed to initiate distortional buckling close to the center of the beam, the boundary conditions for an induced distortional buckling under such circumstances is likely to be at least partially restrained from warping - unlike the case of a simple supported end. The second set of boundary conditions that were considered involved the coupling of a reference node to the rest of the nodes at the ends of the member where the reference node is subjected to rigid rotation, this results in warping fixed ends.

The rigid rotation with respect to the reference node was the boundary condition that was finally adopted in both the local and distortional finite element models

(Figure 6.a &b respectively). Also in both cases, rotation was imposed as prescribed displacement at the reference node to induce uniform moment, resulting in a pin-ended but warping fixed boundary condition.

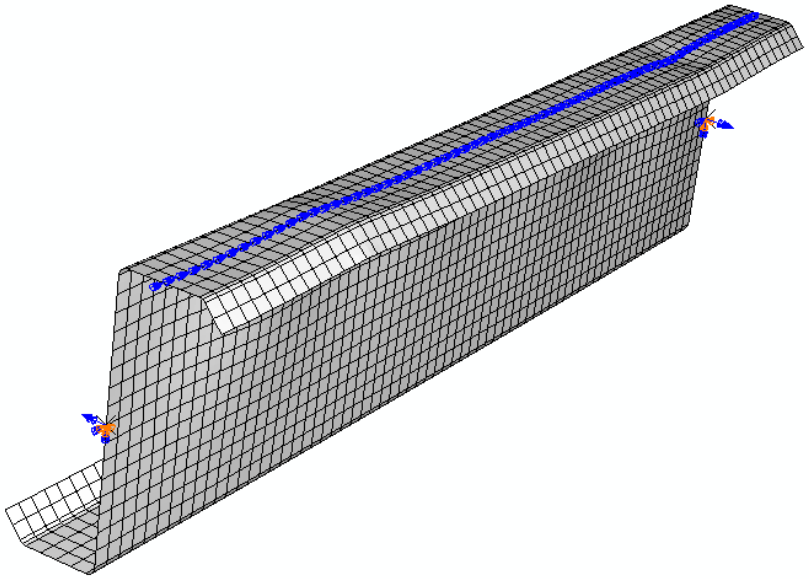

a.

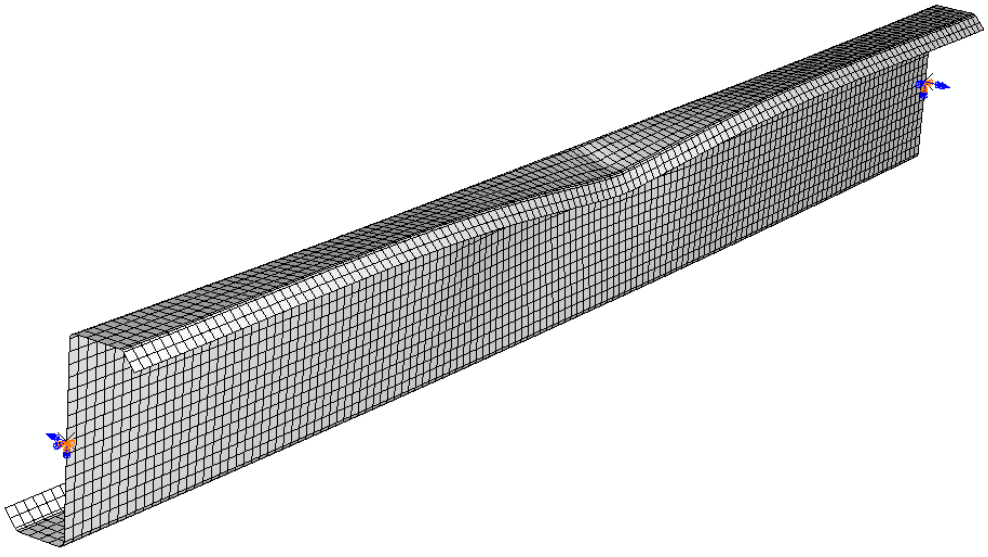

b.

Figure 6 FE model boundary conditions a) Local, b) Distortional

2.5 Imperfections

As the contribution of the geometric imperfections to the study of the non-linear analysis was important, appropriate local and distortional imperfections with three different percentage values (25%, 50% and 75%) with respect to the probability of being exceeded were considered in accordance with that suggested by Schafer and Pekoz (1998). Different modal imperfections were imposed on the members and the models' imperfection sensitivities were analyzed. Local and distortional imperfections that corresponded to the CUFSM elastic local and distortional buckling shapes were adopted. Investigation of imperfection sensitivity was done in the verification and development of the comprehensive study for parametric studies. Two different directions of the imperfections were studied as to their impact on the bending capacity of CFS beams in local and distortional failure.

2.6 Verification of FE Models

A comprehensive verification in the development of a finite element analysis for inelastic bending reserve in cold-formed steel members was examined. The cross-sections that were adopted for verification were tested sections and those studied under the extended FE analysis of the full test set-up that possessed inelastic reserve.

Table 2 shows the comparison of Yu and Shafer (2003, 2006) test results with those from the simplified FE. The results of the finite element analyses showed

that that the percentage difference between the tests and that of the simplified finite element models for failure by local buckling is 3% and for distortional failure with less number of sections falling in this category, 9%. Imperfection magnitude of 50% cdf was adopted for the comparisons of the finite element models. For the simplified model, the length of the member was considered as 64 in. similar to the test set up section where there is a uniform bending moment in the member in the middle 64 in.

The comparison of the extended FE analysis[2] results with those from the simplified FE is shown in Table 3. Various imperfection distribution and magnitudes were considered. For a 50% cdf imperfection magnitude in the case of local buckling failure the results of the finite element analyses showed a 2% difference between the extended and that of the simplified finite element models and a 2% difference in the case of distortional failures. The small percentage differences between the simplified FE models developed and those of the extended FE models indicated that the simple FE models were adequate for capturing the separate test set-ups and the mechanisms associated with local and distortional failures.

[2] In the "extended" FE analysis of Yu and Schafer (2007) the entire test setup is modeled. In the simplified models reported here only the constant moment region is considered.

Table 2 Comparison between tests and simplified FE model with respect to imperfection magnitude

a. Local

Section	f_y (ksi)	M_{test} (kip-in)	M_y (kip-in)	M_{test}/M_y	$M_{fe,loc}$ (kip-in) (25%cdf)	$M_{fe,loc}$ (kip-in) (50%cdf)	$M_{fe,loc}$ (kip-in) (75%cdf)
8.5Z120-2	60.1	280	264	1.06	275.6	266.5	249.8
8C097-3	59.6	172	157	1.10	164.7	156.2	146.3
8C068-5	48.6	104	102	1.02	98.36	94.36	91.37
6C054-2	36.1	45	43	1.06	46.06	42.91	40.02
4C054-2	44.7	28	27	1.03	26.74	25.80	23.37
3.62C054-2	32.0	20	17	1.17	17.36	16.76	15.62

b. Distortional

Section	f_y (ksi)	M_{test} (kip-in)	M_y (kip-in)	M_{test}/M_y	$M_{fe,dist}$ (kip-in) (25%cdf)	$M_{fe,dist}$ (kip-in) (50%cdf)	$M_{fe,dist}$ (kip-in) (75%cdf)
D8.5Z120-4	61.4	254	265	0.96	267.9	263.3	234.8
D8C085-2	52.8	122	124	0.99	112.9	109	103.4
D10C068-4	22.0	51	53	0.95	50.58	48.38	45.90
D3.62C054-3	32.9	17	16	1.04	15.17	15	14.71

Table 3 Extended FE vs. Simplified FE Model with respect to imperfection direction and magnitude

a. Local

Section	f_y (ksi)	$M_{fe,loc,extended}$ (kip-in)	$M_{fe,loc,simplified}$(kip-in)					
			25%		50%		75%	
			Dir1	Dir2	Dir1	Dir2	Dir1	Dir2
8Z2.25x100	33	114.2	118.6	118.8	115.2	115.8	110.1	110.3
8C068	33	69.4	69.25	69.56	67.33	67.50	63.65	63.85
8.5Z082	33	103.2	105.1	105.3	101.7	102.1	96.79	97.3

b. Distortional

Section	f_y (ksi)	$M_{fe,dist,extended}$ (kip-in)	$M_{fe,dist,simplified}$(kip-in)					
			25%		50%		75%	
			Dir1	Dir2	Dir1	Dir2	Dir1	Dir2
8Z2.25x100	33	114.2	113.90	117.1	111.3	115.6	106.9	112
8.5Z092	33	109.5	112.9	115.5	111.3	114.2	108.5	111.4
8.5Z120	44	149.7	155.1	159.1	152.2	158	147.5	153.8
8C097	44	92.3	96.84	97.01	94.64	94.81	89.36	91

2.7 Conclusion

Relatively simple FE models for capturing distinct local and distortional failures were developed, taking into consideration appropriate boundary conditions and other modeling parameters. These models were verified against the test results and extended FE models and were found to be satisfactory. Observation of imperfection sensitivity, primarily with respect to the distortional failures, indicate that imperfection studies need to be accounted for in any parametric analyses to be done later as inelastic bending reserve capacities of CFS beams are investigated.

3. COMPREHENSIVE FINITE ELEMENT STUDY

With the finite element model verified with respect to boundary conditions and other parameters, a comprehensive study needed to be done to understand the behavior of inelastic bending reserve capacity of CFS beams. An investigation into the various parameters involved in coming up with comprehensive FE models that can be adopted for a general study on the inelastic local and distortional bending capacity of beams is discussed in this section.

For a general approach to the problem a fundamental factor that needed to be considered was the choice of appropriate finite element model length in the study of local and distortional buckling effects in inelastic reserve capacity of cold formed steel members subjected to bending. In the non-linear finite element analysis the need to separate the local and distortional buckling modes meant separate member lengths for similar cross-sections so as to simulate the impact of the separation of modes much in the way the tests were set up. In order to accomplish this, different member lengths were considered and the impact of these on the non-linear finite element solutions were compared with the verification test results done by Yu and Schafer (2003, 2006).

3.1 Member Length for Local Finite Element Model

3.1.1 Study of Mesh Density and Imperfection Sensitivity on Member Length Selection

To answer the question of what length of the simplified finite element model should be adopted to predict the inelastic local bending capacities of beams, an investigation into the impact of length variation in local strength prediction is completed. For this study, the seven cross-sections used in the extended finite element studies of Yu and Schafer (2003, 2006) adopted in the previous comprehensive verification (Section 2.6) were considered. A plot of the normalized local failure strength vs. multiples of the critical elastic local buckling half-wave length is shown in Figure 7. The finite element model lengths were varied between 1 to 10 times the critical lengths for the different cross-sections which were computed from an elastic finite strip analysis. Two different mesh densities were considered and as can be seen from Table a (Appendix), there was little or no significant advantage in using the finer mesh case in terms of prediction of local buckling capacities for the various multiples of elastic critical local buckling half-wavelength (n_l) of the finite element model. Hence, the "coarser[3]" mesh was adopted for further investigation of the impact of imperfection direction on failure local bending capacities as a function of model length in terms of the elastic critical local half-wavelength. It can be observed that as those of the verification models (for both tests and extended finite element model study cases of Yu and Schafer (2003, 2006)) with a fixed finite element model, a similar phenomenon was

[3] The "coarse" mesh includes >2 elements in the lip, 4 elements in the flange, and 16 elements in the web; and aspect ratios in accordance with the discussion of Section 2.

observed with respect to imperfection direction sensitivity for a local failure case in that little or no significant change in local capacity prediction was seen for different finite element model lengths as shown in Table a (Appendix). In addition, in Figure 7 it is observed that the local failure moment prediction levels off after a value of n_l=3 for higher multiples of the elastic critical length. This observed convergence of the prediction of local failure moments led to the conclusion that a finite element model that is of length in the neighborhood of three times the cross-sectional elastic critical local half-wavelength can sufficiently predict the inelastic local buckling failure moment capacity of the cross-section. Hence, comprehensive parametric studies that are further discussed will have finite element models of length equal to three times the particular cross-section's elastic critical local half-wavelength.

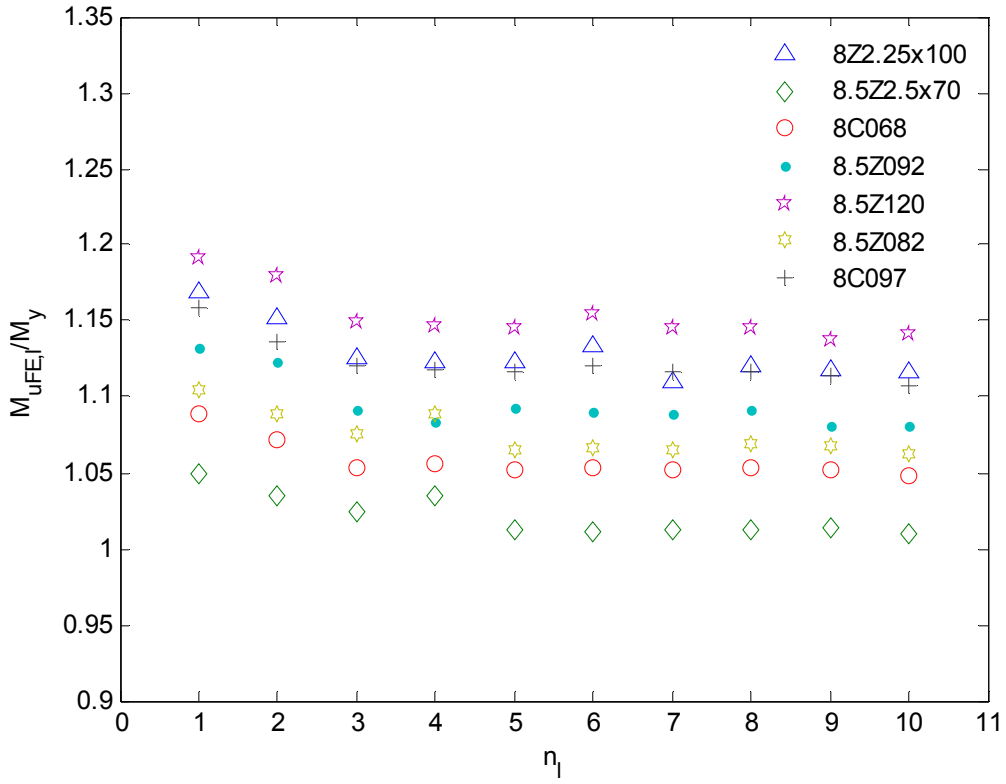

Figure 7 Plot of local FE model length (function of elastic critical length) vs. normalized strength for different sections

3.2 Member Length for Distortional Finite Element Model

3.2.1 Study of Mesh Density and Imperfection Sensitivity on Member Length Selection

In a similar fashion to the case of local buckling, the distortional failure bending capacity ratios normalized with respect to the yield moment were plotted against the finite element model length, normalized in terms of the number of elastic critical distortional bucking half-wave lengths. The seven cross-sections considered in the case of the extended finite element analysis of Yu & Schafer (2003, 2006) were used. The distortional finite element models' length was varied

from 1 to 5 times the elastic critical distortional buckling half-wavelength. Table b (Appendix) shows the impact of mesh density with regards to the failure distortional moment capacities. Two mesh densities were compared and the coarser mesh (same basic mesh density as the “coarser” mesh for the local buckling studies reported in the previous section) was deemed sufficient for further consideration.

The influence of imperfection direction on the distortional failure bending capacities of the finite element models was further investigated with the chosen mesh density. As can be observed in Figure 8, for the various member lengths considered the distortional failure bending capacity was in general sensitive to the imperfection direction, unlike the case of local failure bending capacity.

Two different imperfection sensitivities were observed. The first imperfection direction incorporates a case where the flange at the middle of the member is moving outward. The shape of this imperfection is shown in Figure 9 (b, d & f) where three member lengths with three and five times the elastic critical distortional half-wave lengths for Z and C cross-sections are plotted. The second imperfection direction incorporates a case where the flange at the middle is moving inward. This imperfection direction for the member length with different member lengths is shown in Figure 9 (a, c & e).

The two imperfection directions lead to somewhat different distortional inelastic bending capacities as shown in Figure 8a & b. In the case of the imperfection

where the flange at the middle of the member is moving outward (Figure 9 (b, d & f)) the distortional failure inelastic bending capacities were found to be higher. The inward movement of the flange, on the other hand reduces the inelastic buckling distortional capacity of the member.

As shown in Figure 8a, for the cross-sections considered in the study of member length sensitivity to inelastic distortional bending capacity, about 75% of them exhibited inelastic reserve ($M_{ud}/M_y>1$) for the imperfection direction with middle member flange moving outward. In the second case, where imperfection direction results with middle member flange moving inside, about 90% exhibited inelastic reserve. For a member length with twice the length of the distortional elastic critical buckling half-wave lengths, imperfection direction variation resulted in a maximum of variation of 3.43% in inelastic reserve.

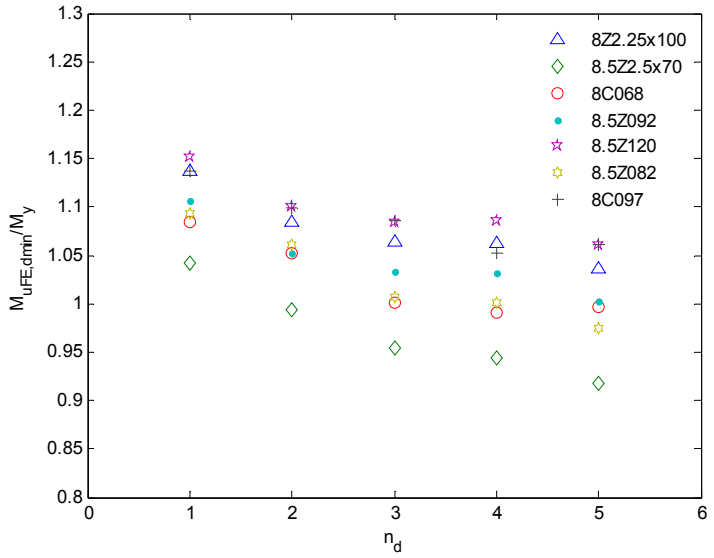

a.

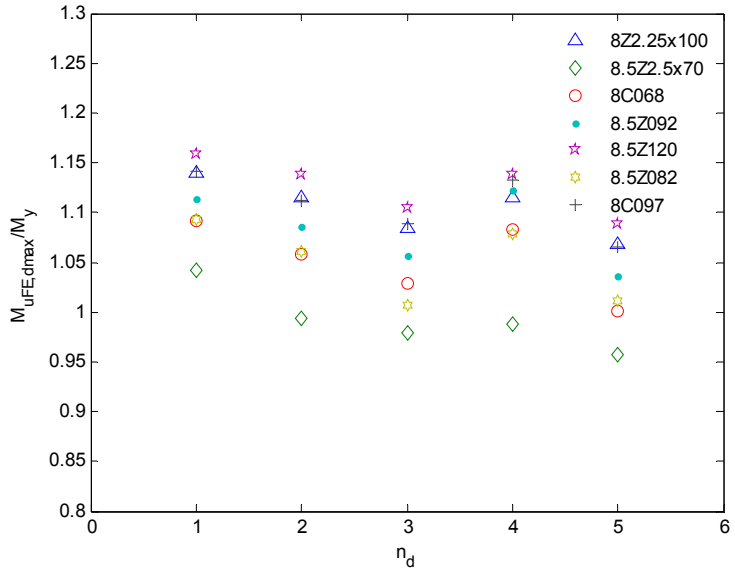

b.

Figure 8 Plot of distortional FE model length (function of elastic critical length) vs. normalized strength for different sections a) Imperfection direction one b) Imperfection direction two

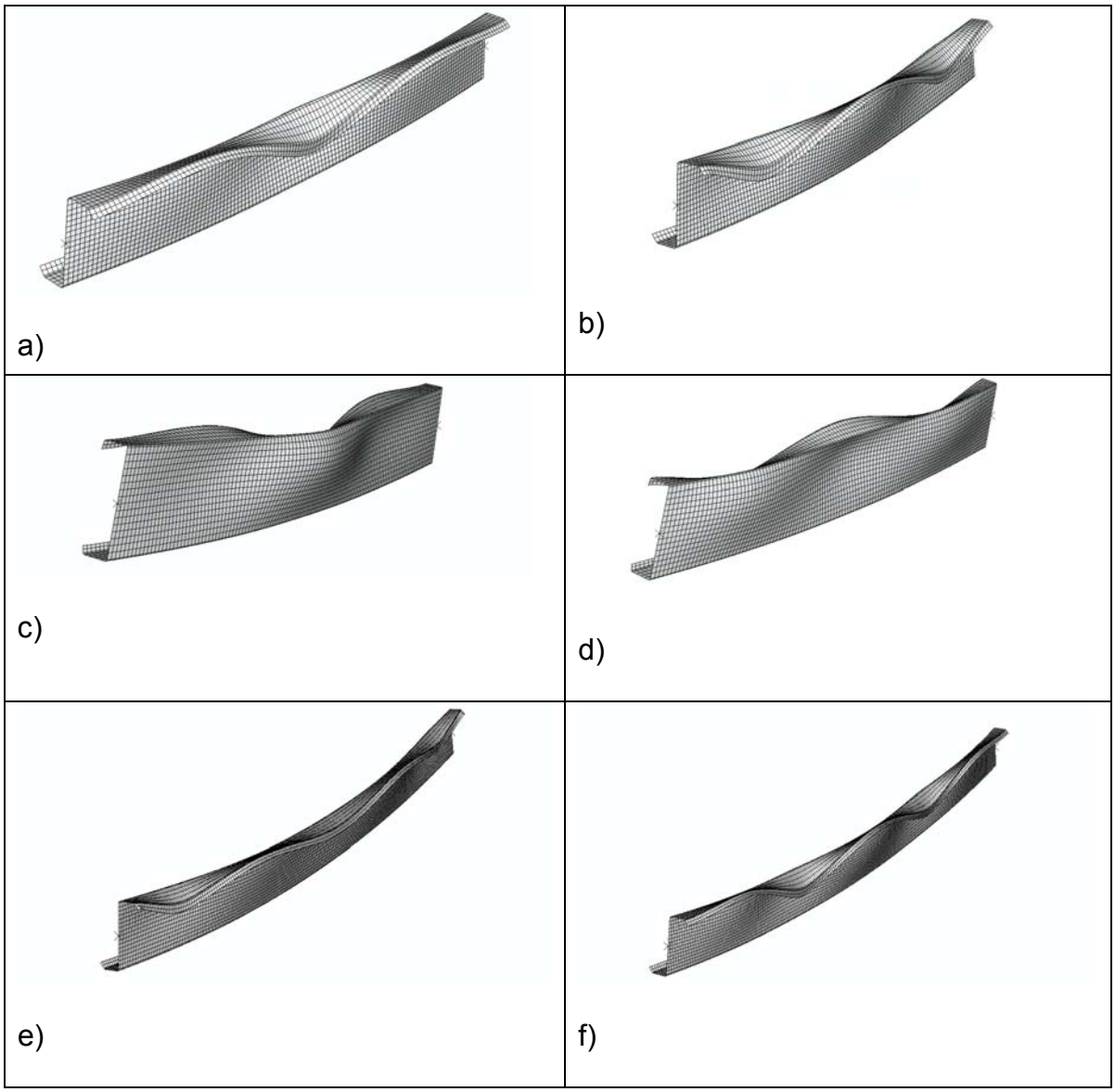

Figure 9 Plot of imperfection direction in distortional buckling failures

a),c),e) inward at mid-span b),d),f) outward at mid-span

3.2.2 Study on the Impact of Lateral-Torsional Buckling in Selection of Member Length for Distortional Models

To decide on the appropriate length of a finite element model that exhibits exclusively distortional failure, the impact of lateral-torsional failure initiation member length is examined. The seven cross-sections used in the extended finite element study of Yu and Schafer that showed inelastic reserve capacities were further analyzed for the effect of lateral-torsional buckling. In order to determine the length of a member to induce lateral torsional buckling the critical elastic lateral-torsional buckling moment is taken as 2.78 M_y or higher since it corresponds to a nominal moment strength of M_α (NAS 2001). Corresponding length of the member that results in such lateral-torsional buckling moment is then determined from classical solutions. These are given in the Table 4.

Table 4 Lateral-torsional buckling length vs. elastic critical distortional length

Section	$L_{cr,d}$ (in)	L^*_{LTB} (in)	$n_{LTB=}$ $L_{LTB}/ L_{cr,d}$
8Z2.25x100	17.5	64.3	3.67
8.5Z2.5x70	22.5	68.1	3.03
8C068	17.5	49.3	2.82
8.5Z092	20.5	67.4	3.29
8.5Z120	18.5	70.4	3.81
8.5Z082	21.5	66.7	3.10
8C097	13.5	48.8	3.61

L_{LTB} = Length at which $M_{cr,e}$= 2.78 M_y for LTB

In Figure 9 the normalized failure load as a function of length of the member in terms of the elastic critical distortional buckling length is plotted along with dashed

lines indicating the break off lengths in terms of the n_d for lateral-torsional failure for the different cross-sections. As can be observed, the lateral-torsional effect starts within a span of member length as a little less than three to around four times the elastic critical distortional half-wavelength. It was hence concluded that in the inelastic bending reserve study for distortional failure bending capacity determination it was satisfactory to adopt a finite element model length twice the critical elastic distortional buckling half-wavelength to observe a distortional failure free of the lateral-torsional buckling effect.

The deformation characteristic for two different member lengths of a section is shown in Figure 11. It is evident from Figure 11a that the member with twice the elastic critical distortional length showed a distortional deformation whereas that with five times the elastic critical distortional length indicated interaction with lateral-torsional buckling (Figure 11 b). It should be noted that the choice of the distortional finite element member length which is the same as the elastic critical distortional length of the cross-section becomes un-conservative. With such length of a member a maximum increase of 5.2% in inelastic capacity was observed in comparison to that of a member length twice the elastic critical distortional length without being unduly influential by the boundary conditions. Hence, a choice of the distortional finite element model length twice the elastic critical distortional length can be considered as appropriate and conservative.

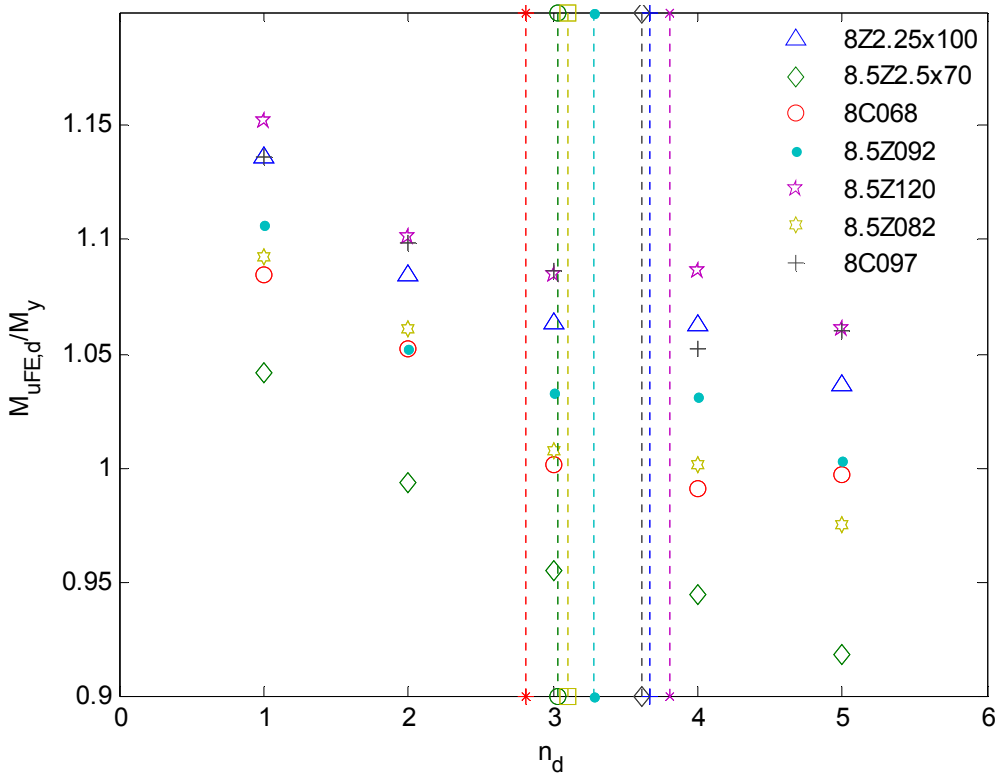

Figure 10 Comparison with distortional buckling models to see break off points where LTB is activated

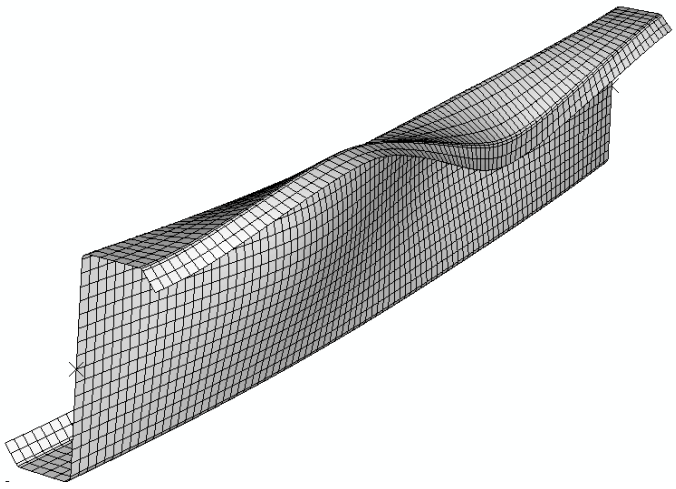

a) $L=2L_{cr,d}$

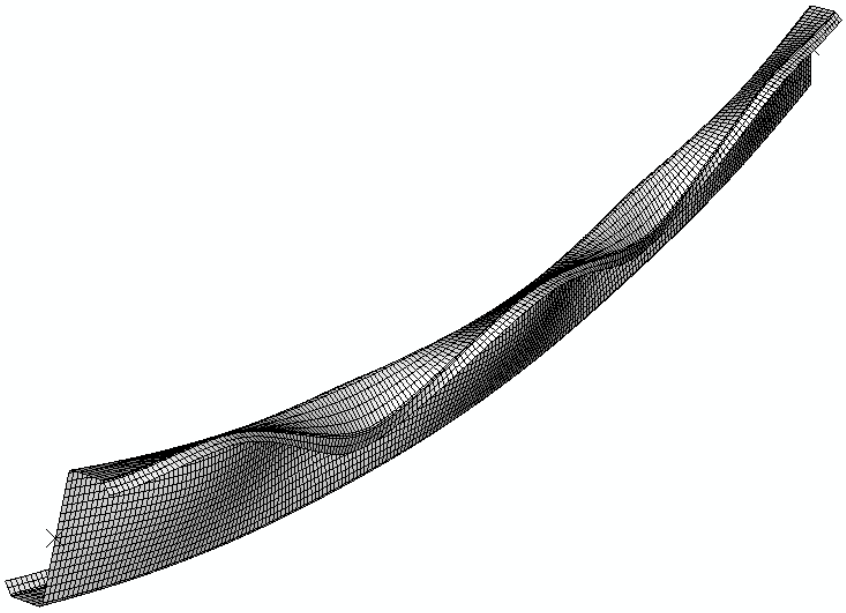

b) $L=5L_{cr,d}$

Figure 11 Deformation plots a) distortional and b) interaction with lateral-torsional buckling

In conclusion, in the preliminary investigation appropriate boundary conditions and mesh densities were considered in coming up with a finite element model that can capture and separate local and distortional failure bending mechanisms. Moreover for a generalized approach to the problem, the inelastic reserve prediction was set up to appropriately capture various cross-sections by making use of the relatively simple finite element model with a length set appropriately as a multiple of the cross-section's critical local or distortional elastic buckling half-wavelength from a finite strip analysis.

4. Parametric Study and Design Formulations

A parametric study considering 17 cross-sections from tests and extended finite element studies of Yu & Schafer (2003, 2006) that exhibited inelastic reserve was done. In order to investigate the phenomenon of inelastic bending reserve in these beams, a range of practical thickness values was made use of to ensure inelastic local and distortional failure bending capacities. These thicknesses ranged from 0.0538 in. to 0.1345 in. and are given in Table C of the Appendix.

An investigation of the impact of strain-hardening and the ultimate stress on the inelastic bending capacity was also done. In order to see this effect, three different variation of the ultimate to yield ratio was considered. Ultimate to yield stress ratios of 1.66 (representing the original tested material model), 1.33 and 1 (representing elastic-perfectly plastic material model) were adopted. The engineering stress-strain curves for the different ultimate to yield stress ratios is shown in Figure 12. The yield stress considered was 33ksi.

In addition, preliminary design expressions are developed based on the experimental data and finite element model results of the parametric study. Possible extension of the current Direct Strength Method to include inelastic reserve is also looked into.

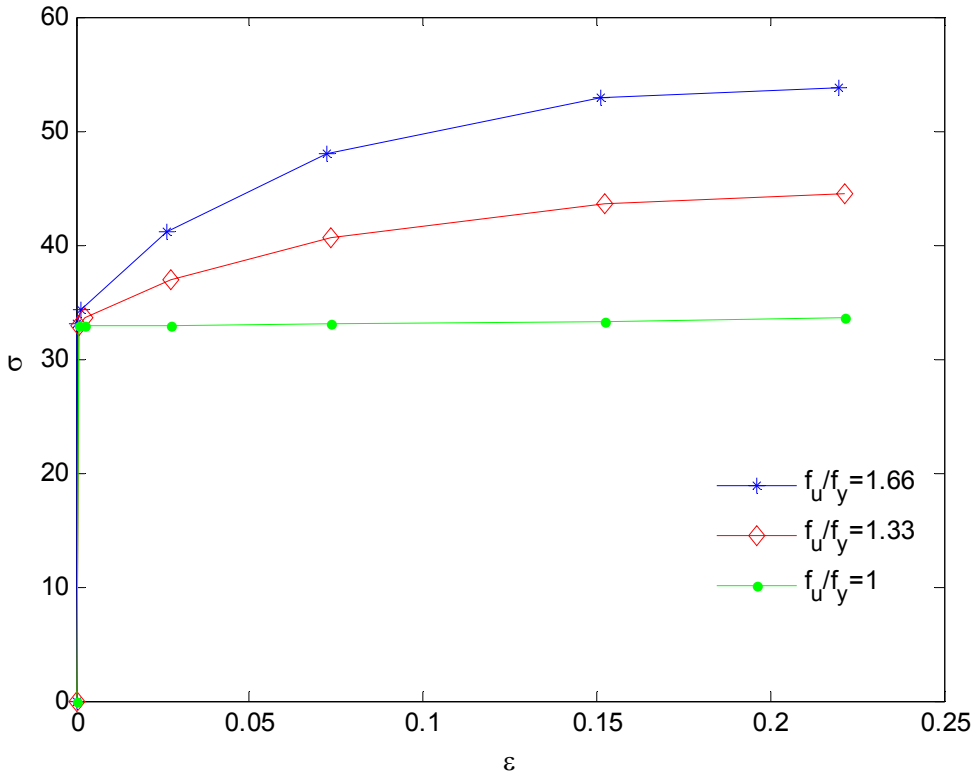

Figure 12 Stress vs. strain for the various f_u/f_y ratios

The finite element models developed for the parametric studies were used in order to examine the impact of a material model's ultimate stress with regards to relationship between strength and strain limits. Cross-section D8.5Z120-4 with eleven thickness variations was selected for this study similar to the parametric study (Table C of Appendix).

4.1 Slenderness vs. Strain Limit Ratio

4.1.1 Parametric Study

Figure 13 shows a plot of slenderness versus the strain limit for the case of distortional and local failure inelastic reserve. The strain limits represent the average membrane strain values at ultimate moments corresponding to either the distortional or the local failure cases. As shown in Figure 13 there was a scatter in the strain limit as a function of slenderness in both cases. The average membrane strain limit reaches as high as 3.5 or 14 times the yield strain for the case of distortional and local buckling failures respectively. It was noted that the higher strains (> 5) in the local buckling cases occurred in the shorter and thicker sections (thickness > 0.10 in.) whose elastic critical local buckling half-wavelengths , hence the finite element model lengths, are shorter. It was observed that using higher multiple (>5) of the local half-wavelengths for generating the finite element models giving longer models in comparison with the section dimensions resulted in reducing these strains.

Computation of C_y from FE models involved FE model lengths that were decided to be a multiple of the critical elastic buckling lengths for local and distortional buckling of the cross-sections; but it was observed that the average compressive strain in the model varied with change in the cross-section length of the FE models, depending on the number of local or distortional buckling waves formed in the post-buckling stability behavior. However the corresponding variation in ultimate inelastic capacity remained basically the same. Hence, this ultimate

reserve capacity was used to back-calculate corresponding strain numerically using the basic mechanics formulations discussed in section 1.2. The back-calculated strain $C_{y,b}$ is hence found to be a practical and general formulation to predict inelastic reserve capacity than $C_{y,FE}$ which was sensitive to assumed length of FE model. Moreover, for tests done in the past that were part of the data for inelastic reserve study in CFS beams, comparison with FE models vis-à-vis normalized strain can be done through $C_{y,b}$ only.

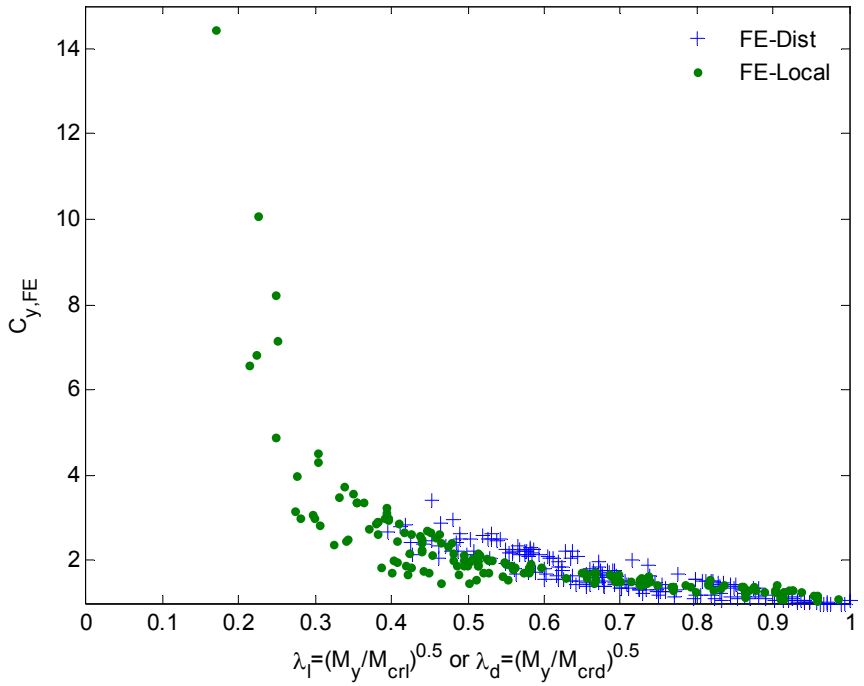

a)

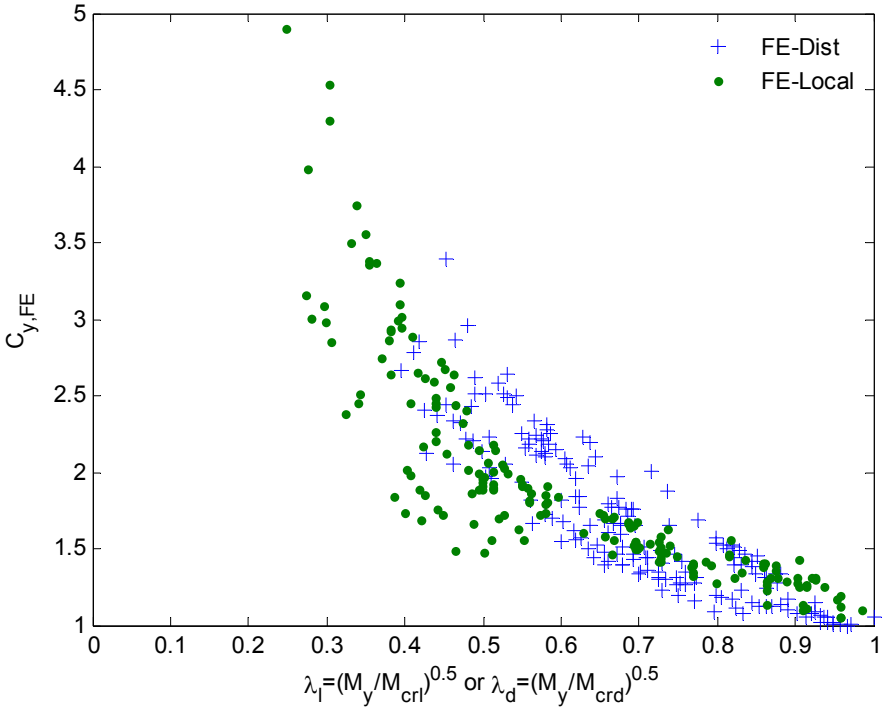

b)

Figure 13 Slenderness vs. normalized strain for FE models a) $C_y \leq 15$

b) Typical C_y

4.1.2 Design

Design expressions that relate elastic buckling slenderness to the membrane strain limit are developed in this section.

A simple power equation was adopted for developing local design equation with lowest sum of squared absolute error as a fitting target. The proposed expression for the local buckling case is given by equation (10) as

if $\lambda_l < \lambda_{ly}$ then $C_{y\ell,FE} = \left(\frac{\lambda_{\ell y}}{\lambda_\ell}\right)^{2.0}$ where λ_{ly}=0.776 & $\lambda_\ell = \sqrt{M_y / M_{cr\ell}}$ (10)

Similarly, for the design equation for a distortional case is given by equation (11):

if $\lambda_d < \lambda_{dy}$ then $C_{yd,FE} = \left(\frac{\lambda_{dy}}{\lambda_d}\right)^{2.5}$ where λ_{dy} =0.673 & $\lambda_d = \sqrt{M_y / M_{crd}}$ (11)

Using back-calculated strain, the relation between strain and slenderness two relationships (equations 12 & 13 for local and distortional cases respectively) are developed. With data corresponding to f_u/f_y of 1.66, same as tested cross-section material model, these relationships become:

if $\lambda_l < \lambda_{ly}$ then $C_{y\ell_b} = \left(\frac{\lambda_{\ell y}}{\lambda_\ell}\right)^{0.544}$ where λ_{ly} =0.776 & $\lambda_\ell = \sqrt{M_y / M_{cr\ell}}$ (12)

if $\lambda_d < \lambda_{dy}$ then $C_{yd_b} = \left(\frac{\lambda_{dy}}{\lambda_d}\right)^{0.983}$ where λ_{dy} =0.673 & $\lambda_d = \sqrt{M_y / M_{crd}}$ (13)

The design expressions given by equations (12 & 13) are found to be conservative in comparison with the available test data. A plot of the proposed design curves is shown in Figure 14 along with tests and FE model results.

The variation of local and distortional slenderness with strain-limits for the different ultimate to yield stress ratios is also shown in Figure 14. The variation in the prediction of the membrane strain limit for the distortional case shows a sharp increase as the distortional slenderness values get smaller. For the majority of the cross-sectional thicknesses considered the variation of strain limit prediction was not varying significantly in the case of distortional failures. The local failures exhibited more scatter in the membrane strain limit predictions in contrast to the distortional failures. This variation for the different ultimate to yield stress was more

distinct for thicker cross-sections. Expressions relating the slenderness variation with strain limits for these data points were developed in various forms as shown in equations 14-16.

$$\text{if } \lambda_l < \lambda_{ly} \text{ then } C_{y\ell b} = \left(\frac{\lambda_{\ell y}}{\lambda_\ell}\right)^{0.4615\frac{M_p}{M_y}\frac{f_u}{f_y}} \text{ where } \lambda_{ly}=0.776 \text{ \& } \lambda_\ell = \sqrt{M_y/M_{cr\ell}} \qquad (14)$$

Since M_p/M_y for the section is the same and also since it is included in the M_u/M_y prediction equation as one factor, a more appropriate expression could be:

$$\text{if } \lambda_l < \lambda_{ly} \text{ then } C_{y\ell b} = \left(\frac{\lambda_{\ell y}}{\lambda_\ell}\right)^{0.543\frac{f_u}{f_y}} \text{ where } \lambda_{ly}=0.776 \text{ \& } \lambda_\ell = \sqrt{M_y/M_{cr\ell}} \qquad (15)$$

Ignoring the impact of f_u/f_y gives equation (16):

$$\text{if } \lambda_l < \lambda_{ly} \text{ then } C_{y\ell b} = \left(\frac{\lambda_{\ell y}}{\lambda_\ell}\right)^{0.721} \text{ where } \lambda_{ly}=0.776 \text{ \& } \lambda_\ell = \sqrt{M_y/M_{cr\ell}} \qquad (16)$$

Comparison of equation (16) with the expression developed with $f_u/f_y=1.66$ (equation 12) for the parametric study indicates that equation (12) is a more conservative equation as shown in Figure 14 a.

Similarly the distortional relationships corresponding to the various cases leading to development of equations 14-16 are given in equations 17-19:

$$\text{if } \lambda_d < \lambda_{dy} \text{ then } C_{yd\,b} = \left(\frac{\lambda_{dy}}{\lambda_d}\right)^{0.84\frac{M_p}{M_y}\frac{f_u}{f_y}} \text{ where } \lambda_{dy}=0.673 \text{ \& } \lambda_d = \sqrt{M_y/M_{crd}} \qquad (17)$$

$$\text{if } \lambda_d < \lambda_{dy} \text{ then } C_{yd\,b} = \left(\frac{\lambda_{dy}}{\lambda_d}\right)^{0.989\frac{f_u}{f_y}} \text{ where } \lambda_{dy}=0.673 \text{ \& } \lambda_d = \sqrt{M_y/M_{crd}} \qquad (18)$$

if $\lambda_d < \lambda_{dy}$ then $C_{yd\,b} = \left(\frac{\lambda_{dy}}{\lambda_d}\right)^{1.3}$ where λ_{dy} =0.673 & $\lambda_d = \sqrt{M_y / M_{crd}}$ (19)

Similar comparison of equation (19) with equation (13) for the parametric study data indicates that equation (13) is conservative as shown in Figure 14 b. Figure 14 c shows both the local and distortional design curves via equations (13) and (19) respectively.

The relationship between slenderness and C_y was based on slenderness values the correspond to M_{cr} as a result of elastic stress distribution despite the fact that C_y is essentially due to the inelastic stress distribution. This becomes even more significant for smaller slenderness values with high C_y. Slenderness that is function of M_{cr} which takes into factor inelastic stress distribution might explain the scatter in the plots relating slenderness and C_y observed in Figure 14. Previously this was investigated in part by calculating M_{cr} for the inelastic stress distribution, although the differences were not great they did exist and were dependent on the cross-section, or more exactly the influence of the web on the local buckling mode, since the web sees the changing stress distribution (from elastic to inelastic).

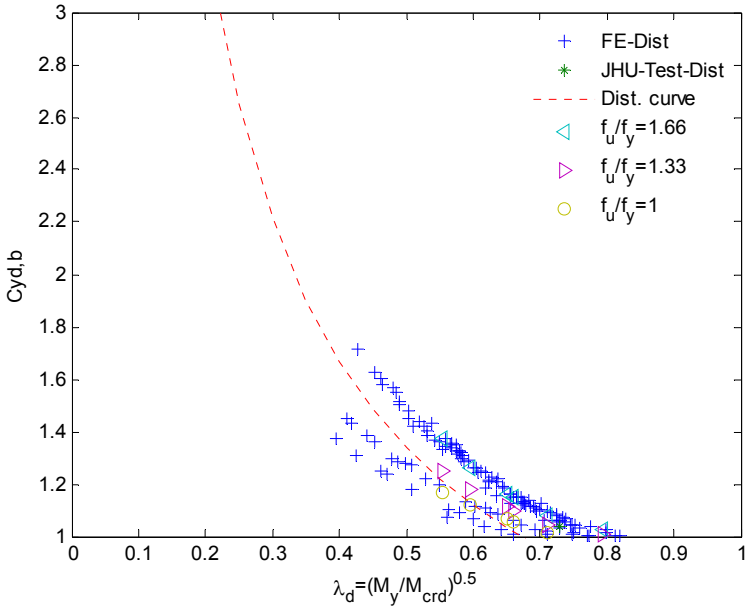
FE-Dist
JHU-Test-Dist
Dist. curve
f_u/f_y=1.66
f_u/f_y=1.33
f_u/f_y=1
Cyd,b
$\lambda_d=(M_y/M_{crd})^{0.5}$

a)

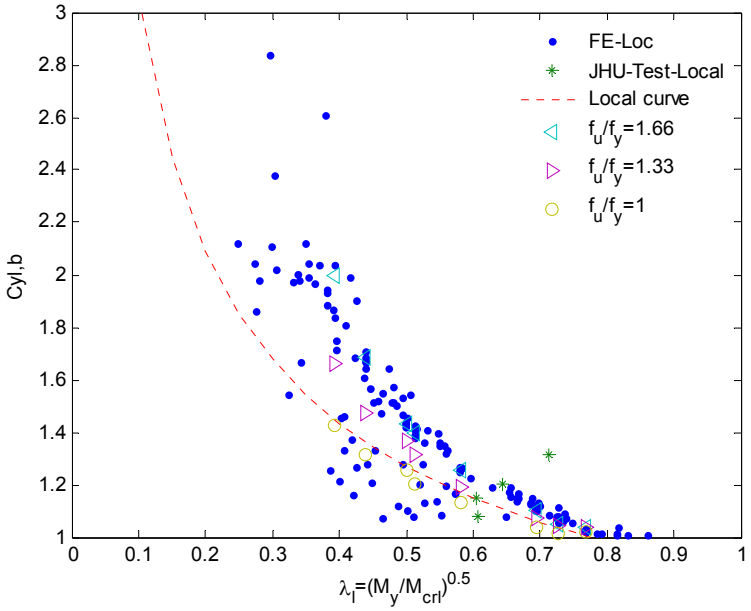
FE-Loc
JHU-Test-Local
Local curve
f_u/f_y=1.66
f_u/f_y=1.33
f_u/f_y=1
Cyl,b
$\lambda_l=(M_y/M_{crl})^{0.5}$

b)

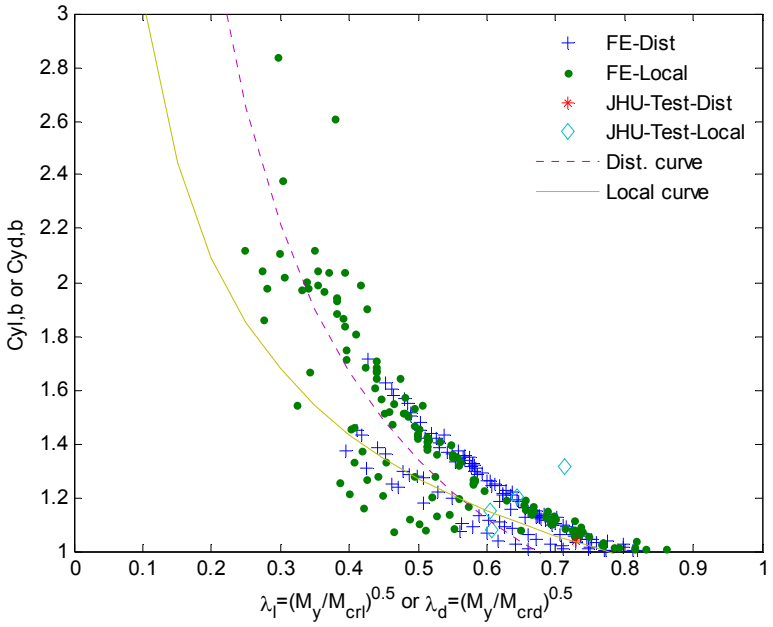

c)

Figure 14 Slenderness vs. back-calculated normalized strain for test & FE models & proposed design curve a) Distortional b) Local c) Both local and distortional

4.2 Strain Limit vs. Strength

4.2.1 Parametric Study

The variation of average membrane normalized finite element strain-limit ($C_{y,FE}$) as a function of normalized strength prediction is shown in Figure 15. In both the distortional and local failures, as the average membrane strain increases the normalized strength prediction increases. Both the distortional and local failure strength prediction plots indicate scatter. It was noted that the maximum average membrane strain was found to be higher for local failures than for distortional failures. For a typical normalized strength prediction, it can be observed that the

typical average membrane strain limits ($C_{y,FE}$) fall under 4 for the case of distortional failures and under 5 for the case of local failures.

4.2.2 Design

The proposed design equation relating the average normalized strain-limit to normalized moment for the local and distortional cases is given by equation (20) and shown in Figure 15.

$$\frac{M_n - M_y}{M_p - M_y} = 1 - \left(\frac{1}{C_{y,FE}} \right)^{0.75} \quad \text{for } C_{y,FE}>1 \tag{20}$$

Using back-calculated strain-limit, the equation for strength prediction is given by equation (21):

$$\frac{M_n - M_y}{M_p - M_y} = 1 - \left(\frac{1}{C_{yb}} \right)^{2.42} \quad \text{for } C_{yb}>1 \tag{21}$$

Figure 16 shows the normalized strength vs. back-calculated strain limit for both local and distortional failures for the parametric study FE models, tests along with the results for the study for different material models, and the proposed design curve. It can be observed that the back-calculated strain- slenderness relationship equation fits well with the FE and test results.

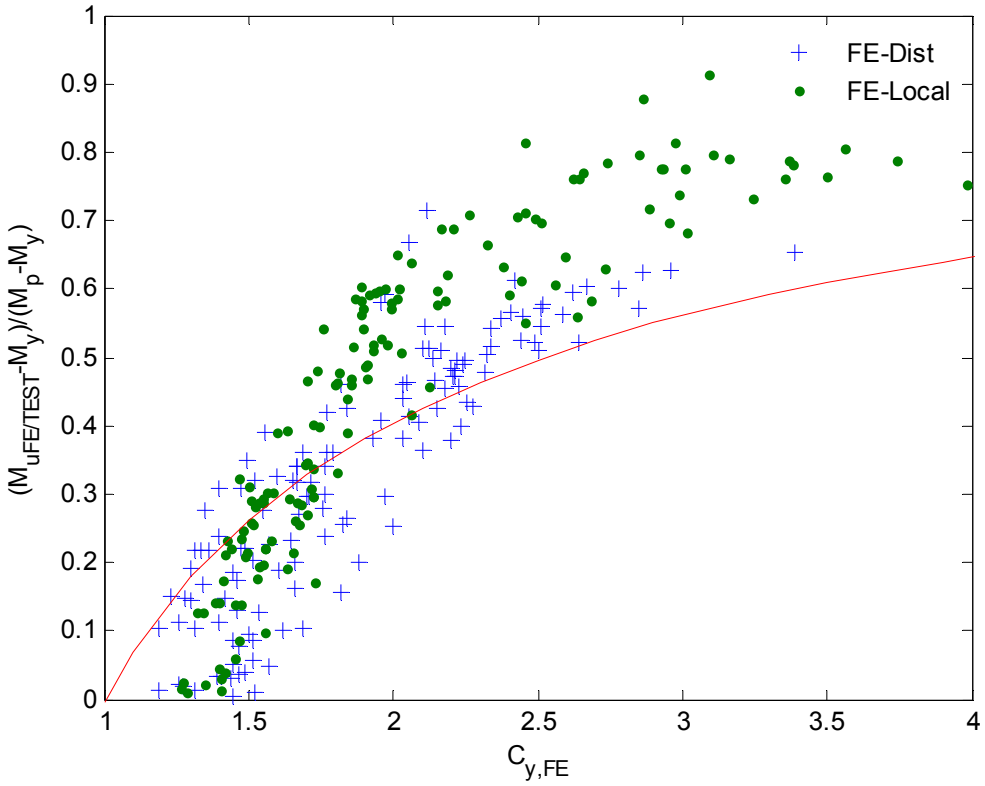

Figure 15 Normalized strain vs. strength for FE models & design curve

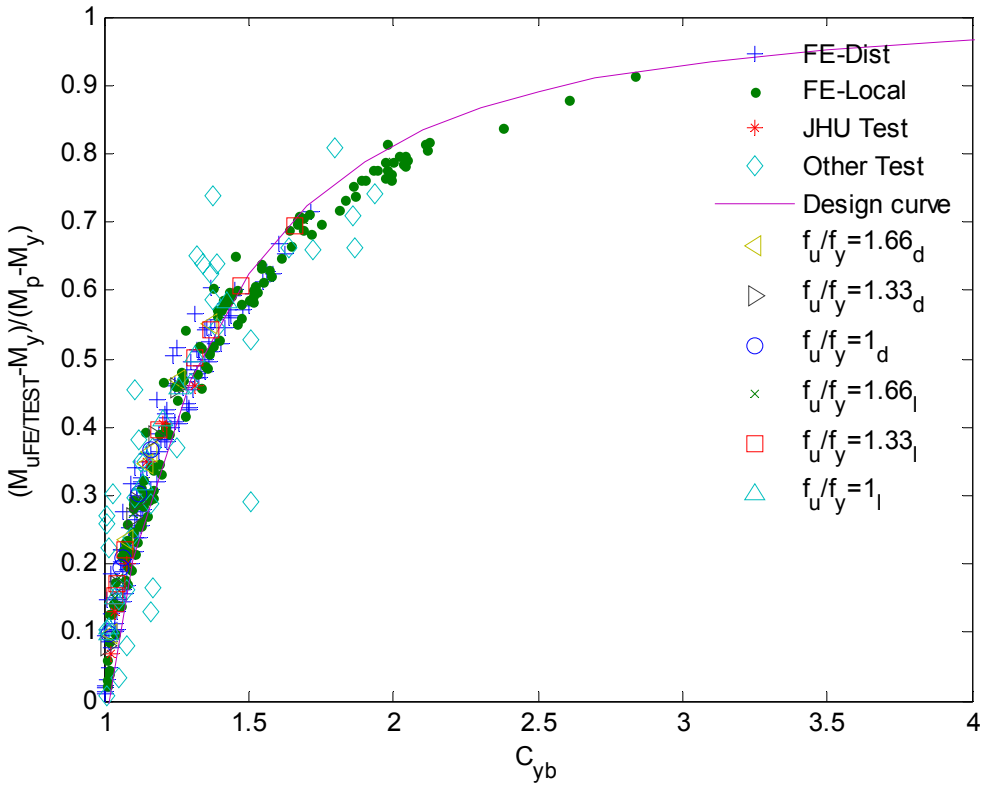

Figure 16 Back-calculated normalized strain vs. strength for test, FE models & design curve

4.3 Direct Strength Method Formulation: Slenderness as a Function of Strength

4.3.1 Parametric Study

Figure 17 shows a study of the distortional strength predictions which are normalized with respect to the yield and plastic strengths, as a function of the slenderness of the cross-section. Among the 187 finite element models, 72% of those with distortional boundary conditions and 77% of the models with local boundary conditions possessed inelastic reserve.

4.3.2 Design

Design expressions relating slenderness and bending strength are developed in this section. Equations (12) & (21) were combined to give the expression for local strength prediction given in equation (22)

$$\text{If } \lambda_l < \lambda_{ly},\ M_{n\ell} = M_y + \left(M_p - M_y\right)\left(1 - \left(\frac{\lambda_\ell}{\lambda_{\ell y}}\right)^{1.32}\right) \qquad (22)$$

Similarly, for distortional strength prediction the expression developed by combining equations (13) and (21) is given by equation (23)

$$\text{If } \lambda_d < \lambda_{dy},\ M_{nd} = M_y + \left(M_p - M_y\right)\left(1 - \left(\frac{\lambda_d}{\lambda_{dy}}\right)^{2.38}\right) \qquad (23)$$

The curves using these expressions are shown in Figure 17 plotted against the distortional and local finite element data points and test results and extended FE results of Yu and Schafer.

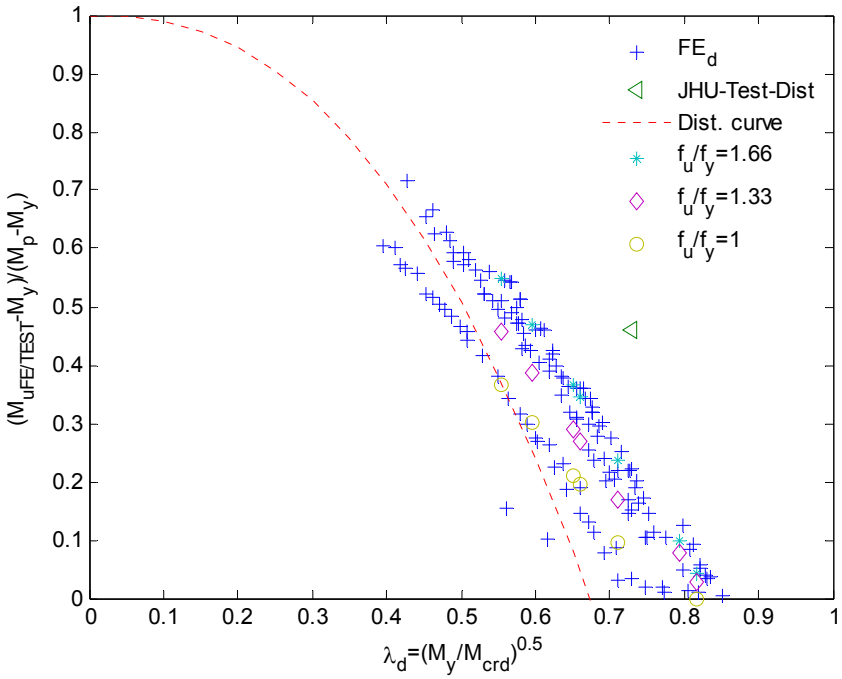

a)

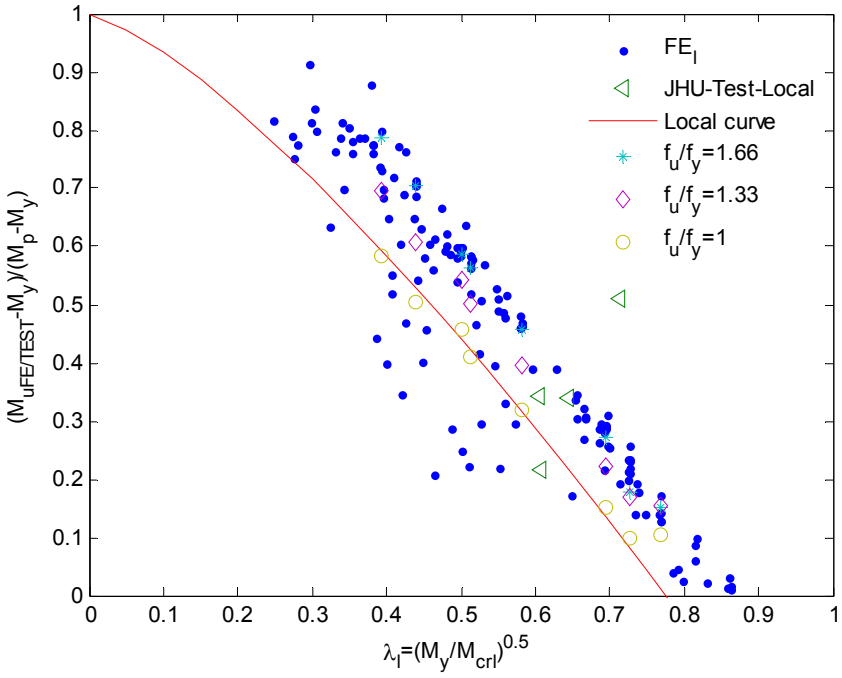

b)

Figure 17 Slenderness vs. strength for test & FE models & proposed design curve

a) Distortional b) Local

4.3.3 Design Statistics

The statistics using the Direct Strength Method prediction formulations for inelastic bending reserve capacity is shown in Table 5 for the data that included the tests and finite element models. The DSM prediction equations correspond well with observed results from tests and are with reasonably low standard deviations.

Table 5 Prediction statistics for inelastic bending capacity

Section and	Mtest/Mn			Mtest/Mn for Mn>My*		
Researcher	ave.	st.dev.	n	ave.	st.dev.	n
Hats and Decks						
Acharya (1997)	1.11	0.08	12	1.03	0.01	2
Desmond (1977)	1.10	0.03	2			
Hoglund (1980)	1.05	0.07	36	1.00	0.04	15
Papazian (1994)	1.17	0.16	8	0.98	0.03	2
C and Z 's						
Cohen (1987)	1.18	0.07	7			
LaBoube and Yu (1978)	1.14	0.04	10			
Rogers (1995)	1.05	0.05	17	1.04	0.04	12
Shan (1994)	1.11	0.09	6	1.15	0.02	3
Yu and Schafer (2003)	1.03	0.04	8	1.04	0.04	6
Yu and Schafer (2006)	1.08	0.02	4			
All test data	1.08	0.09	110	1.03	0.06	40
FE Studies						
Local models	1.03	0.03	187	1.02	0.02	135
Distortional models	1.06	0.05	187	1.05	0.04	144

* these statistics are provided only when Eq. 14 and 15 are employed for prediction, i.e., when the predicted Mn is greater than My (or equivalently $\lambda_{\ell}<\lambda_{\ell y}$ or $\lambda_{d}<\lambda_{dy}$)

5. APPENDIX

Table A Study of length of simplified local FE model

Mesh 1 +50%

Section	Mfe,loc,extended (kip-in)	Mfe,loc,simplified(kip-in)									
		n_l=									
		1	2	3	4	5	6	7	8	9	10
8Z2.25x100	114.2	124.60	122.50	119.7	119.2	119.3	119.3	118.0	119.3	119	118.7
8.5Z2.5x70	87.9	91.51	89.92	89.02	89.80	88.08	88.23	88.04	88.59	88.50	87.95
8C068	69.4	71.28	69.97	68.67	68.77	68.63	68.62	68.73	68.82	68.68	68.56
8.5Z092	117.2	121.90	119.80	118.20	118.60	117.50	117.2	117.5	117.6	117.6	117.6
8.5Z120	155.6	169.8	166.6	163.7	163.8	163.5	163.4	163.4	163.3	163.3	162.8
8.5Z082	103.2	108.1	106.9	104.3	103.4	104.3	104.0	104.1	104.3	103.4	103.4
8C097	98.1	105.6	103.4	101.40	100.5	100.8	100.9	100.8	100.4	100.7	100.5

Mesh2 +50%

Section	$M_{fe,loc,extended}$ (kip-in)	$M_{fe,loc,simplified}$(kip-in)									
		n_l=									
		1	2	3	4	5	6	7	8	9	10
8Z2.25x100	114.2	124.1	122.4	119.5	119.2	119.2	120.4	117.9	119.0	118.7	118.6
8.5Z2.5x70	87.9	91.13	89.82	88.90	89.84	87.85	87.78	87.89	87.88	88.00	87.69
8C068	69.4	70.95	69.84	68.70	68.81	68.56	68.70	68.57	68.66	68.63	68.33
8.5Z092	117.2	122.3	121.3	117.9	117.0	118.0	117.7	117.6	117.9	116.8	116.8
8.5Z120	155.6	169.9	168.2	163.9	163.5	163.4	164.6	163.4	163.4	162.2	162.8
8.5Z082	103.2	107.1	105.6	104.3	105.6	103.3	103.4	103.3	103.7	103.6	103.0
8C097	98.1	104.4	102.4	101.0	100.7	100.6	100.9	100.6	100.6	100.3	99.73

Mesh 2 -50%

Section	$M_{fe,loc,extended}$ (kip-in)	$M_{fe,loc,simplified}$(kip-in)									
		n_l=									
		1	2	3	4	5	6	7	8	9	10
8Z2.25x100	114.2	123.6	121.4	119.3	119.4	119.0	119.2	119.0	119.0	118.8	118.4
8.5Z2.5x70	87.9	91.72	90.87	88.60	87.63	88.54	88.28	88.75	88.42	87.96	89.35
8C068	69.4	70.72	69.56	68.63	68.61	68.40	68.23	68.41	68.38	68.49	68.22
8.5Z092	117.2	121.6	119.7	118	118.6	117.2	117.2	117.2	117.3	117.3	116.6
8.5Z120	155.6	169.2	166.4	163.5	163.8	163.3	162.9	163.1	162.9	162.8	162.3
8.5Z082	103.2	107.7	107.0	104.2	103.1	103.9	103.6	104.0	103.7	103.2	103
8C097	98.1	104.4	102.4	101.0	100.7	100.6	100.9	100.6	100.6	100.3	99.73

Table B Study of length of simplified distortional FE model

Mesh 1 +50%

Section	$M_{fe,dist,extended}$ (kip-in)	$M_{fe,dist,simplified}$(kip-in)				
		n_d=				
		1	2	3	4	5
8Z2.25x100	114.2	120.8	115.3	115.2	118.3	110.1
8.5Z2.5x70	81.7	90.55	85.94	84.99	85.88	79.71
8C068	63.7	70.75	68.99	65.53	64.45	65.05
8.5Z092	109.5	120.1	117.4	111.6	111.4	111.9
8.5Z120	149.7	164.40	157.00	157.60	162.10	151.00
8.5Z082	94.8	106.00	102.90	97.78	97.16	98.09
8C097	92.3	103.00	99.16	98.08	101.00	96.33

Mesh2 +50%

Section	$M_{fe,dist,extended}$ (kip-in)	$M_{fe,dist,simplified}$(kip-in)				
		n_d=				
		1	2	3	4	5
8Z2.25x100	114.2	120.7	115.2	115.2	118.4	110.1
8.5Z2.5x70	81.7	90.39	86.20	85.02	85.72	79.65
8C068	63.7	70.70	68.97	65.29	64.58	65.02
8.5Z092	109.5	119.5	113.6	114.1	121.2	108.3
8.5Z120	149.7	165.2	162.4	154.7	154.9	155.2
8.5Z082	94.8	106.0	102.9	97.72	97.16	98.05
8C097	92.3	102.8	99.00	97.89	102.0	96.02

Mesh 2 -50%

Section	$M_{fe,dist,extended}$ (kip-in)	$M_{fe,dist,simplified}$(kip-in)				
		n_d=				
		1	2	3	4	5
8Z2.25x100	114.2	121.0	118.4	113.0	112.9	113.4
8.5Z2.5x70	81.7	90.39	86.20	82.88	81.94	83.12
8C068	63.7	71.21	68.60	67.11	70.57	65.25
8.5Z092	109.5	120.3	117.3	111.6	111.4	111.9
8.5Z120	149.7	164.3	157	157.5	162.4	151.3
8.5Z082	94.8	106.0	102.9	97.72	104.6	94.57
8C097	92.3	102.4	100.2	98.08	94.80	95.54

Table C Parametric study

Section	t (in.)	M_y (kip-in)	M_p (kip-in)	$M_{fe,loc}$ (kip-in) (+50%cdf)	$M_{fe,dist}$ (kip-in) (+50%cdf)	$M_{fe,dist}$ (kip-in) (-50%cdf)
8Z2.25x100	0.0538	58.66	68.70	57.76	53.94	56.35
8Z2.25x100	0.0566	61.71	72.28	61.5	59.88	57.91
8Z2.25x100	0.0598	65.20	76.36	65.45	64.10	62.46
8Z2.25x100	0.0673	73.38	85.94	75.62	72.89	74.08
8Z2.25x100	0.0713	77.74	91.05	81.14	79.67	78.39
8Z2.25x100	0.0747	81.45	95.39	85.68	82.91	84.10
8Z2.25x100	0.0897	97.80	114.55	105.8	104.7	101.8
8Z2.25x100	0.1017	110.89	129.87	121.9	117.8	120.5
8Z2.25x100	0.1046	114.05	133.57	125.8	124.3	121.5
8Z2.25x100	0.1196	130.40	152.73	145.8	144.7	141.1
8Z2.25x100	0.1345	146.65	171.76	166.4	160.7	164.5
8.5Z2.5x70	0.0538	67.25	78.58	63.09	59.37	62.74
8.5Z2.5x70	0.0566	70.75	82.67	68.62	63.97	66.97
8.5Z2.5x70	0.0598	74.74	87.34	73.62	71.65	69.41
8.5Z2.5x70	0.0673	84.12	98.29	84.76	81.65	83.01
8.5Z2.5x70	0.0713	89.12	104.14	91.22	87.88	89.39
8.5Z2.5x70	0.0747	93.37	109.10	96.42	94.64	93.51
8.5Z2.5x70	0.0897	112.12	131.01	119.5	117.9	115.2
8.5Z2.5x70	0.1017	127.12	148.54	138	136.5	133.1
8.5Z2.5x70	0.1046	130.74	152.77	142.2	137.3	141
8.5Z2.5x70	0.1196	149.49	174.68	165.8	159.8	164.3
8.5Z2.5x70	0.1345	168.11	196.44	189	182.2	187.5
8C068	0.0538	50.37	60.01	50.05	50.61	48.72
8C068	0.0566	52.99	63.13	53.29	52.29	53.76
8C068	0.0598	55.99	66.70	57.05	57.19	56.21
8C068	0.0673	63.01	75.07	65.8	65.73	65.43
8C068	0.0713	66.76	79.53	70.53	70.02	70.56
8C068	0.0747	69.94	83.32	74.58	74.11	74.08
8C068	0.0897	83.98	100.05	92.48	90.95	91.71
8C068	0.1017	95.22	113.43	105.9	105.5	104.5
8C068	0.1046	97.93	116.67	110.4	108.9	107.7

8C068	0.1196	111.98	133.40	128.5	126.2	124.7
8C068	0.1345	125.93	150.02	146.1	141.7	142.9
8.5Z092	0.0538	65.30	77.03	63.32	59.22	62.51
8.5Z092	0.0566	68.70	81.04	66.7	63.84	66.68
8.5Z092	0.0598	72.58	85.62	72.79	71.25	69.08
8.5Z092	0.0673	81.69	96.36	83.57	82.63	80.96
8.5Z092	0.0713	86.54	102.08	89.83	87.12	88.75
8.5Z092	0.0747	90.67	106.95	95.35	92.20	93.93
8.5Z092	0.0897	108.87	128.43	117.9	113.2	116.9
8.5Z092	0.1017	123.44	145.61	136.1	135.2	130.7
8.5Z092	0.1046	126.96	149.76	140.5	135.2	139.3
8.5Z092	0.1196	145.16	171.24	163.5	157.2	162.1
8.5Z092	0.1345	163.25	192.57	186	179.2	184.8
8.5Z120	0.0538	66.96	78.78	63.36	65.56	60.16
8.5Z120	0.0566	70.45	82.88	67.85	67.69	64.74
8.5Z120	0.0598	74.43	87.56	73.18	72.41	70.11
8.5Z120	0.0673	83.77	98.54	85.86	84.06	82.15
8.5Z120	0.0713	88.75	104.40	92.19	88.49	90.32
8.5Z120	0.0747	92.98	109.38	97.73	93.92	95.58
8.5Z120	0.0897	111.65	131.34	120.8	118.9	115.6
8.5Z120	0.1017	126.58	148.91	139.5	133.2	137.5
8.5Z120	0.1046	130.19	153.16	143.8	137.5	142.2
8.5Z120	0.1196	148.86	175.12	167.4	159.9	165.5
8.5Z120	0.1345	167.41	196.94	189.9	182.6	188
8.5Z082	0.0538	65.27	77.21	63.95	59.21	62.52
8.5Z082	0.0566	68.67	81.23	68.35	63.84	66.66
8.5Z082	0.0598	72.55	85.82	72.5	71.21	69.07
8.5Z082	0.0673	81.65	96.59	84.23	80.93	82.63
8.5Z082	0.0713	86.50	102.33	90.58	88.71	87.05
8.5Z082	0.0747	90.63	107.21	95.5	92.04	93.97
8.5Z082	0.0897	108.83	128.74	118.4	116.9	113.2
8.5Z082	0.1017	123.39	145.96	136.6	131.1	134.7
8.5Z082	0.1046	126.90	150.12	140.8	135.3	139.2
8.5Z082	0.1196	145.10	171.65	163.9	162.2	157.4
8.5Z082	0.1345	163.18	193.03	186.7	179.4	184.8

8C097	0.0538	49.94	59.89	49.37	48.74	48.10
8C097	0.0566	52.54	63.01	52.68	51.77	52.04
8C097	0.0598	55.51	66.57	56.47	56.14	55.66
8C097	0.0673	62.48	74.92	65.15	64.30	65.09
8C097	0.0713	66.19	79.38	69.96	69.51	69.08
8C097	0.0747	69.34	83.16	74.01	73.23	73.16
8C097	0.0897	83.27	99.86	91.74	89.90	90.23
8C097	0.1017	94.41	113.22	105.8	103.3	103.9
8C097	0.1046	97.10	116.45	109.3	106.6	107.4
8C097	0.1196	111.03	133.15	127.2	124.7	123.5
8C097	0.1345	124.86	149.74	144.9	140.5	142.8
8.5Z120-2	0.0538	66.00	77.71	64.26	59.05	62.05
8.5Z120-2	0.0566	69.43	81.75	68.72	63.66	66.31
8.5Z120-2	0.0598	73.36	86.37	73.67	68.92	70.99
8.5Z120-2	0.0673	82.56	97.21	84.62	81.07	82.57
8.5Z120-2	0.0713	87.46	102.98	91.08	87.53	88.71
8.5Z120-2	0.0747	91.63	107.89	96.2	92.28	94
8.5Z120-2	0.0897	110.03	129.56	119	113.4	117.1
8.5Z120-2	0.1017	124.75	146.89	137.2	135.2	131.4
8.5Z120-2	0.1046	128.31	151.08	141.6	139.8	135.6
8.5Z120-2	0.1196	146.71	172.74	164.6	162.7	157.8
8.5Z120-2	0.1345	164.99	194.27	187.7	185.5	180.0
8C097-3	0.0538	49.99	59.80	49.17	47.81	48.36
8C097-3	0.0566	52.59	62.91	52.43	51.43	51.75
8C097-3	0.0598	55.56	66.47	56.21	55.93	55.28
8C097-3	0.0673	62.53	74.81	64.96	64.77	63.93
8C097-3	0.0713	66.25	79.25	69.66	69.21	68.73
8C097-3	0.0747	69.40	83.03	73.54	73.01	72.38
8C097-3	0.0897	83.34	99.70	91.34	89.53	89.89
8C097-3	0.1017	94.49	113.04	105.5	102.9	103.6
8C097-3	0.1046	97.18	116.27	108.9	106.2	107.0
8C097-3	0.1196	111.12	132.94	126.8	123.0	124.3
8C097-3	0.1345	124.97	149.50	143.7	142.2	140.0
8C068-5	0.0538	49.98	59.73	48.53	47.28	47.31
8C068-5	0.0566	52.58	62.83	51.77	51.13	50.71

8C068-5	0.0598	55.55	66.39	55.46	54.22	55.47
8C068-5	0.0673	62.52	74.71	64.21	64.18	62.75
8C068-5	0.0713	66.24	79.15	69.03	67.59	68.59
8C068-5	0.0747	69.40	82.93	73.06	72.29	71.69
8C068-5	0.0897	83.33	99.58	90.08	88.78	88.51
8C068-5	0.1017	94.48	112.90	104.8	103.0	102.3
8C068-5	0.1046	97.17	116.12	108.2	105.3	105.5
8C068-5	0.1196	111.11	132.77	125.9	122.4	123.6
8C068-5	0.1345	124.95	149.31	143.5	140.1	139
6C054-2	0.0538	33.53	39.43	35.36	34.14	35.67
6C054-2	0.0566	35.27	41.49	37.28	36.21	37.95
6C054-2	0.0598	37.27	43.83	39.83	40.43	38.61
6C054-2	0.0673	41.94	49.33	45.75	44.22	46.35
6C054-2	0.0713	44.44	52.26	48.9	47.17	49.58
6C054-2	0.0747	46.55	54.75	51.78	49.75	52.11
6C054-2	0.0897	55.90	65.75	63.41	64.03	60.94
6C054-2	0.1017	63.38	74.54	73.17	69.85	73.36
6C054-2	0.1046	65.19	76.67	74.23	71.99	75.75
6C054-2	0.1196	74.54	87.66	84.41	83.29	87.32
6C054-2	0.1345	83.82	98.58	95.88	94.37	99.49
4C054-2	0.0538	19.28	21.97	19.87	21.05	19.36
4C054-2	0.0566	20.29	23.12	21.13	22.79	20.51
4C054-2	0.0598	21.43	24.42	22.17	21.82	24.66
4C054-2	0.0673	24.12	27.49	25.47	24.88	27.72
4C054-2	0.0713	25.56	29.12	27.23	30.28	26.52
4C054-2	0.0747	26.78	30.51	28.72	31.63	27.89
4C054-2	0.0897	32.15	36.63	35.28	34.01	37.61
4C054-2	0.1017	36.45	41.53	40.5	38.91	44.28
4C054-2	0.1046	37.49	42.72	41.75	45.32	40.08
4C054-2	0.1196	42.87	48.85	49.49	46.20	51.36
4C054-2	0.1345	48.21	54.93	56.66	52.25	58.47
3.62C054-2	0.0538	17.20	19.61	18.15	19.11	17.47
3.62C054-2	0.0566	18.10	20.63	19.28	20.44	18.47
3.62C054-2	0.0598	19.12	21.80	20.57	22.14	19.62
3.62C054-2	0.0673	21.52	24.53	23.15	24.64	22.35

3.62C054-2	0.0713	22.80	25.99	24.73	26.33	23.81
3.62C054-2	0.0747	23.89	27.23	26.06	25.03	27.64
3.62C054-2	0.0897	28.69	32.70	31.95	33.96	30.46
3.62C054-2	0.1017	32.52	37.08	37.24	39.10	34.82
3.62C054-2	0.1046	33.45	38.13	37.73	35.87	40.07
3.62C054-2	0.1196	38.25	43.60	44.62	46.53	41.28
3.62C054-2	0.1345	43.01	49.03	49.96	46.65	52.51
D8.5Z120-4	0.0538	65.81	77.43	62.45	60.10	63.38
D8.5Z120-4	0.0566	69.24	81.46	67.01	67.58	64.68
D8.5Z120-4	0.0598	73.15	86.06	73.27	72.14	69.92
D8.5Z120-4	0.0673	82.33	96.86	84.19	83.68	81.90
D8.5Z120-4	0.0713	87.22	102.61	90.84	89.73	87.99
D8.5Z120-4	0.0747	91.38	107.51	96.03	93.41	94.89
D8.5Z120-4	0.0897	109.73	129.09	118.8	117.8	114.6
D8.5Z120-4	0.1017	124.41	146.36	137.2	131.9	136.2
D8.5Z120-4	0.1046	127.96	150.54	141.5	140.7	136.1
D8.5Z120-4	0.1196	146.31	172.13	164.7	158.2	163.5
D8.5Z120-4	0.1345	164.53	193.57	187.7	186.6	180.4
D8C085-2	0.0538	50.85	60.82	49.92	48.71	50.08
D8C085-2	0.0566	53.50	63.99	53.2	52.32	53.30
D8C085-2	0.0598	56.53	67.60	56.98	56.86	56.66
D8C085-2	0.0673	63.61	76.08	66	65.41	65.96
D8C085-2	0.0713	67.40	80.60	70.78	70.26	70.66
D8C085-2	0.0747	70.61	84.45	74.87	74.60	73.90
D8C085-2	0.0897	84.79	101.41	92.89	91.53	91.58
D8C085-2	0.1017	96.13	114.97	107.4	105.5	105.2
D8C085-2	0.1046	98.87	118.25	110.9	108.5	108.9
D8C085-2	0.1196	113.05	135.21	128.5	125.7	126.3
D8C085-2	0.1345	127.14	152.05	146.6	143.1	142.7
D10C068-4	0.0538	69.17	84.83	61.55	58.03	60.11
D10C068-4	0.0566	72.77	89.24	65.84	64.32	62.17
D10C068-4	0.0598	76.88	94.29	71.22	69.65	66.88
D10C068-4	0.0673	86.52	106.11	82.84	81.41	77.71
D10C068-4	0.0713	91.66	112.42	90.03	83.96	87.96
D10C068-4	0.0747	96.04	117.78	95.62	88.31	92.78

D10C068-4	0.0897	115.32	141.43	119.8	115.6	111.2
D10C068-4	0.1017	130.75	160.35	139.5	130.4	134.8
D10C068-4	0.1046	134.48	164.93	144.6	138.0	133.1
D10C068-4	0.1196	153.76	188.58	169.7	162.2	157.3
D10C068-4	0.1345	172.92	212.07	194.5	184.3	179.0
D3.62C054-3	0.0538	16.21	18.42	16.7	16.14	18.27
D3.62C054-3	0.0566	17.05	19.38	17.72	17.13	19.11
D3.62C054-3	0.0598	18.02	20.47	18.53	18.23	20.62
D3.62C054-3	0.0673	20.28	23.04	21.23	20.80	23.63
D3.62C054-3	0.0713	21.48	24.41	22.65	22.16	25.01
D3.62C054-3	0.0747	22.51	25.57	23.86	23.32	25.71
D3.62C054-3	0.0897	27.03	30.71	29.36	28.43	32.13
D3.62C054-3	0.1017	30.64	34.82	33.88	35.93	32.55
D3.62C054-3	0.1046	31.52	35.81	34.91	38.36	33.52
D3.62C054-3	0.1196	36.04	40.95	41.29	38.61	43.07
D3.62C054-3	0.1345	40.53	46.05	49.16	43.68	49.48

ACKNOWLEDGMENTS

This material is based upon work supported by the National Science Foundation under Grant No. 0448707. Any opinions, findings, and conclusions or recommendations expressed in this material are those of the authors and do not necessarily reflect the views of the National Science Foundation.

REFERENCES

ABAQUS (2007) ABAQUS/Standard User's Manual, Version 6.7, ABAQUS, Inc., Pawtucket, RI, www.abaqus.com

Acharya, V.V., Schuster, R.M. (1998). "Bending Tests of Hat Section with Multiple Longitudinal Stiffeners." Proceedings of the Fourteenth International Specialty Conference on Cold-Formed Steel Structures, October 1998, St. Louis, Missouri, 77-92.

Bambach, M. R., Rasmussen, K. J. R. (2004). "Design Provisions for Sections Containing Unstiffened Elements with Stress Gradient." ASCE, Journal of Structural Engineering. 130 (10) 1620–1628.

Camotim, D., Silvestre, N., Dinis, P.B., Bebiano, R., Basaglia, C. (2006). "Recent progress on the numerical analysis of thin-walled steel members and frames." Proceedings of the International Symposium on Innovative Design of Steel Structures, 10 November 2006, Hong Kong, Ed. B. Young, 63-104.

Cohen, J. M. (1987). "Local Buckling Behavior of Plate Elements." Department of Structural Engineering Report, Cornell University, Ithaca, New York.

Desmond, T.P. (1977). "The Behavior and Design of Thin-Walled Compression Elements with Longitudinal Stiffeners." Ph.D. Thesis, Cornell University, Ithaca, New York.

Höglund, T. (1980). "Design of Trapezoidal Sheeting Provided with Stiffeners in the Flanges and Webs." Swedish Council for Building Research, Stockholm, Sweden, D28:1980.

LaBoube, R.A., Yu, W., (1978). "Structural Behavior of Beam Webs Subjected to Bending Stress." Civil Engineering Study Structural Series, 78-1, Department of Civil Engineering, University of Missouri-Rolla, Rolla, Missouri.

NAS (2001). North American Specification for the Design of Cold-Formed Steel Structural Members. American Iron and Steel Institute, Washington, D.C. (Also Canadian Standards Association CSA S136-01)

NAS (2004). Supplement 2004 to the North American Specification for the Design of Cold-Formed Steel Structural Members 2001 Edition: Appendix 1, Design of Cold-Formed Steel Structural Members Using Direct Strength Method. American Iron and Steel Institute, Washington, D.C.

Papazian, R.P., Schuster, R.M., Sommerstein, M. (1994). "Multiple Stiffened Deck Profiles." Proceedings of the Twelfth International Specialty Conference on Cold-Formed Steel Structures, October 1994, St. Louis, Missouri, 217-228.

Reck, H.P., Peköz,T.; Winter,G. (1975). "Inelastic strength of cold-formed steel beams." ASCE, Journal of the Structural Division, 101 (11) 2193-2203.

Rogers, C.A. (1995). "Interaction Buckling of Flange, Edge Stiffener and Web of C-Sections in Bending." M.S. Thesis, University of Waterloo, Ontario, Canada.

Schafer, B.W. (2006). “Review: The Direct Strength Method of Cold-Formed Steel Member Design.” Proceedings of International Colloquium on Stability and Ductility of Steel Structures, Lisbon, Portugal, Ed. Camotim et al., Vol. 1, 49-66.

Schafer, B.W., Ádány, S. (2006). “Buckling analysis of cold-formed steel members using CUFSM: conventional and constrained finite strip methods.” Proceedings of the Eighteenth International Specialty Conference on Cold-Formed Steel Structures, October 2006, Orlando, Florida. 39-54.

Schafer, B.W., Peköz, T. (1998). “Computational Modeling of Cold-Formed Steel: Characterizing Geometric Imperfections and Residual Stresses.” Elsevier, Journal of Constructional Steel Research. 47 (3) 193-210.

Shan, M., R.A. LaBoube, W. Yu, (1994). “Behavior of Web Elements with Openings Subjected to Bending, Shear and the Combination of Bending and Shear.” Civil Engineering Study Structural Series, 94-2, Department of Civil Engineering, University of Missouri-Rolla, Rolla, Missouri.

Yener, M., Peköz, T. (1983). “Limit design in cold-formed steel.” ASCE, Journal of Structural Engineering, 109 (9) 2033-2047.

Yener, M., Peköz, T. (1983). “Partial Stress Redistribution in Cold-Formed Steel.” ASCE, Journal of Structural Engineering, 111 (6) 1169-1185.

Yu, C., Schafer, B.W. (2003). “Local Buckling Tests on Cold-Formed Steel Beams.” ASCE, Journal of Structural Engineering. 129 (12) 1596-1606.

Yu, C., Schafer, B.W. (2006). “Distortional buckling tests on cold-formed steel beams.” ASCE, Journal of Structural Engineering. 132 (4) 515-528.

Yu, C., Schafer, B.W. (2007). “Simulation of Cold-Formed Steel Beams in Local and Distortional Buckling with Application to the Direct Strength Method” Elsevier, Journal of Constructional Steel Research 63 (5) 581-590.